IS-T--1820

Neutron Scattering Studies of the RENi*2*B*2*C (RE=LU, Y, Ho, Er): Lattice Dynamics

by

Bullock, Max

PHD Thesis submitted to Iowa State University

Ames Laboratory, U.S. DOE
Iowa State University
Ames, Iowa 50011

Date Transmitted: February 23, 1998

PREPARED FOR THE U.S. DEPARTMENT OF ENERGY
UNDER CONTRACT NO. W-7405-Eng-82.

DISCLAIMER

DISCLAIMER

TABLE OF CONTENTS

* Removed for separate processing —

* Removed for separate processing

LIST OF FIGURES

LIST OF TABLES

ACKNOWLEDGMENTS

The author would like to thank his advisor Professor C. Stassis for his guidance and support. Special thanks are also extended to Professor P.C. Canfield and Dr. B.K. Cho for growing excellent single crystals which were used in the experiments for this dissertation.

The author would also like to thank Dr. J. Zarestky, Prof. B.N. Harmon, Prof. A. Goldman, Dr. P. Dervenagas, Prof. W. Weber, Dr. Gen Shirane, Dr. S.M. Shapiro, and Mr. Z. Honda for their assistance during the course of this work. I would also like to thank my fiancee for giving me support.

The assistance and hospitality of the Neutron Scattering Groups at Oak Ridge National Laboratory and Brookhaven National Laboratory is greatly appreciated.

Finally, appreciation is extended to the many people at Iowa State University and Ames Laboratory who create an excellent scientific environment.

This work was performed at Ames Laboratory under Contract No. W-7405-Eng-82 with the U.S. Department of Energy. The United States government has assigned the DOE Report number IS-T 1820 to this dissertation.

CHAPTER 1. INTRODUCTION

Background-General

Superconductivity and magnetic order are two fundamental properties of matter that have been studied for decades. However, few materials exhibit both properties. The first such systems were made by introducing magnetic impurities into superconducting materials.[1,2] These systems gave great insight into the pair-breaking mechanisms of the magnetic impurities of these superconductors. However, magnetic ions would interact and destroy the superconductivity before enough of the ions had been added to the system to order magnetically.

In the 1970's, two systems were discovered that allowed for the study of the interaction between superconductivity and magnetic ordering. These two systems were the $REMo_6(S,SE)_8$, and $RERh_4B_4$ (where RE stands for a rare-earth element)[2] which are superconducting ternary compounds[3,4,5]. From these two systems, it was concluded that superconductivity can coexist with long range antiferro-magnetic order, but that ferromagnetism usually leads to the destruction of superconductivity[2-15]. Experimentally, these systems are hard to study because T_N(i.e. magnetic transition

temperatures) is very low; (≤1K) which is below the temperature of pumped liquid ^{4}He. Also $T_c >> T_N$ for most of these systems. Therefore you cannot examine comparable energy scales. In addition single crystal samples were very rare and not examined until 5-10 years after the discovery of a new system.

$RENi_2B_2C$-Introduction

The recent discovery of the rare-earth boride carbide family $RENi_2B_2C$ [16,17,18,19] has provided another system to study the interplay of superconductivity and magnetism. In addition, these compounds have much higher transition temperatures ($T_N \approx 1.5$-20K, $T_c \approx 6.2$-16.6K) which make them easier to work with experimentally. This system exhibits a variety of ground states from just superconductivity (in *Y*[20,21] and *Lu* compounds), superconductivity coexisting with magnetic order (*Tm*[22], *Er*[23], *Ho*[24], and *Dy*[25,26] compounds), and magnetic order without superconductivity (*Gd*[27] and *Tb*[28] compounds). The transition temperatures for these compounds are given in Table 1.1[29], with the highest superconducting temperatures, 16.6 and 15.6K for the Lu and Y compounds. The superconductors in these compounds are conventional superconductors even though they have a layered structure,

Table 1.1: Transition temperatures of the $RENi_2B_2C$ family.

RE	T_c(K)	T_N(K)
Y[21]	15.5	-
Lu[17]	16.6	-
Tm[22]	10.8	1.5
Er[23]	10.5	6
Ho[23]	8.5	6
Dy[25]	6.2	10
Tb[28]	-	15
Gd[27]	-	20
Sm[29]	-	9
Nd[29]	-	4.5

common to high T_c superconductors, which can be seen in Figure 1.1.

Incommensurate Magnetic Structure

Many interesting papers have been published on the $RENi_2B_2C$ system since the discovery of these compounds in 1994. Of particular relevance to this dissertation is the magnetic structure of a few of the magnetic compounds, specifically the magnetic ordering of Ho, Er, Gd, and Tb. These compounds order in an incommensurate modulation of the moments along **a*** with wave vectors of 0.585, 0.553, 0.553, and 0.551 to 0.545 for Ho[30,31,32], Er[33,34], Gd[35], and Tb[36], respectively. In Er (T_c = 10.5K), below 6 K, magnetic diffraction peaks appear in rows parallel to the reciprocal a-axis as in Figure 1.2. These peaks can be indexed as first and higher-order satellites of the allowed nuclear reflections with an incommensurate wave vector (0.553,0,0). A similar magnetic structure with wave vector (0.585,0,0) was also observed between approximately 6 and 4.7 K in the Ho compound.

It is interesting that an incommensurate magnetic structure with wave vector along **a*** is a common feature of the magnetic structures of several of these compounds(Ho, Er, Tb, and Gd). The magnitude of the wave vectors do not vary appreciably among these compounds and are close to the zone

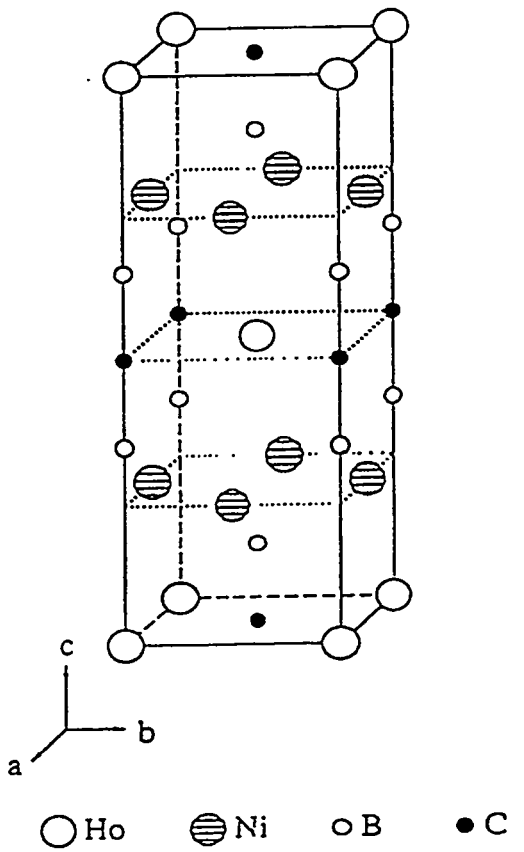

Figure 1.1: The crystal structure of $HoNi_2B_2C$. Ho can be replaced with any rare-earth element. (After Reference Grigereit[31])

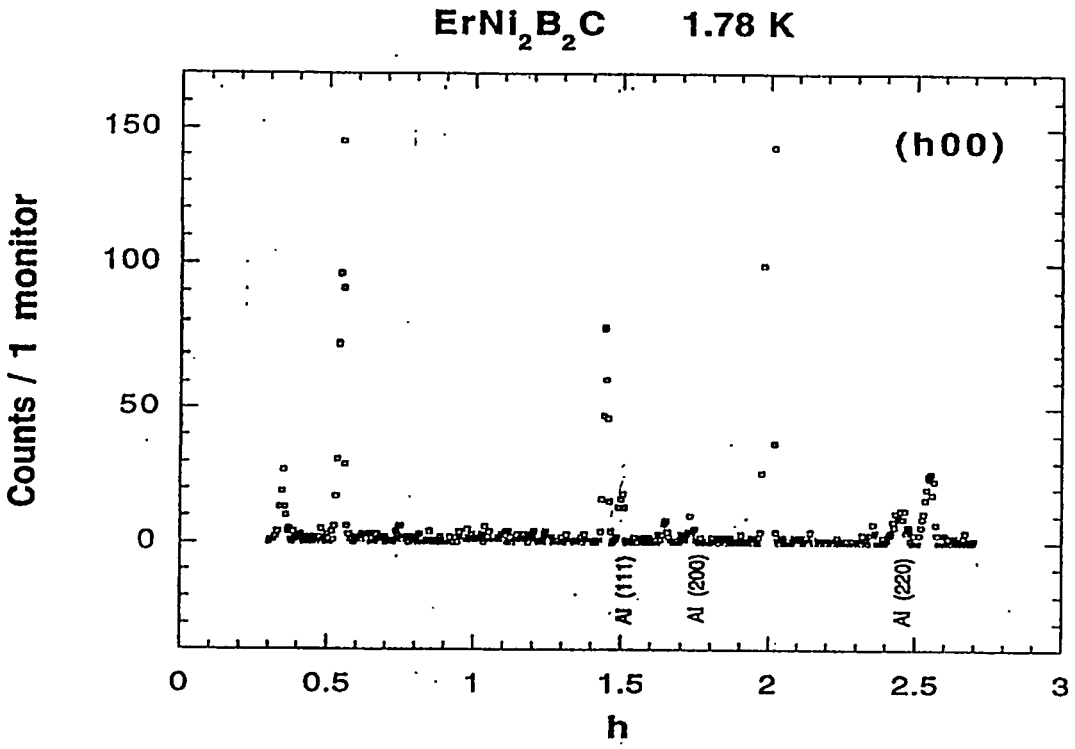

Figure 1.2: Neutron diffraction scan along the **a*** direction for $ErNi_2B_2C$. One monitor corresponds to a counting interval of approximately 1 sec. (After reference Zarestky[29])

boundary point G_1. This suggests that there are common Fermi surface nesting features along **a*** which cause the magnetic ordering of the rare-earth magnetic moments via the Ruderman-Kittel-Kasuya-Yosida (RKKY) mechanism.[37,38,39,40]

Phonon Softening-Kohn Anomaly

The lattice vibrations of the atoms are partly screened by the electrons. Essentially, a phonon of wave vector $\vec{q}$ and frequency ω sets up a potential field due to the motion of the ions in the metal. The electrons move to screen this field and modify the ion-ion interaction which in turn alters the phonon frequency. The screened field will be inversely proportional $\varepsilon(\vec{q})$, where $\varepsilon(\vec{q})$ is the dielectric function describing the screening of the electrons(see appendix A). By modifying the forces between the ions, the lattice frequency, ω, of this mode of vibration will depend on $\varepsilon(\vec{q})$. Hence, any singularity in ε will be reflected in the phonon frequency.[41]

Kohn[42] proposed that for metals this screening changes rather rapidly, depending on the Fermi surface's geometry. Thus, the electron-phonon interaction will be reflected in the phonon spectrum of some metals depending on the detailed electronic structure. In addition, $\varepsilon(\vec{q})$ will change when $\vec{q}$ is equal to a spanning vector connecting two pieces of Fermi

surface. This means that the electrons which usually screen the motions of the ions are unable to screen as effectively for $\vec{q} = \vec{q}_{ext}$, where $\vec{q}_{ext}$ is a q vector connecting two extremum pieces of Fermi surface. Kohn was the first person to point out that the drop in $\varepsilon(\vec{q})$ as $\vec{q}$ is increased through $\vec{q}_{ext}$, where $\vec{q}_{ext} = 2\vec{k}_f$ for a free electron gas with Fermi wave number $\vec{k}_f$, should lead to a small sudden change in the eigenfrequency $\omega(\vec{q})$ at the point $\vec{q} = \vec{q}_{ext}$.

This effect of the electron-phonon interaction on the phonon dispersion curves was first observed by Brockhouse[43] in lead. The dispersion curves of lead have several small anomalous kinks at wave vectors corresponding to nested pieces of the fermi surface. Since this time, numerous Kohn anomalies have been observed in other metals.

A calculation(without matrix elements) of the generalized electronic susceptibility $\chi(q)$, where

$$\varepsilon(\vec{q}) = 1 + 4\pi\chi(\vec{q}),$$

is shown in Figure 1.3. This electronic susceptibility for $LuNi_2B_2C$ is based on the normal-state electronic band structure of this compound which was made by Rhee et al.[44] The $\chi(q)$ showed a peak near wave vectors corresponding to those observed for the incommensurate magnetic structure observed in Ho, Er, Gd, and Tb. This peak in $\chi(q)$ is due to a nesting of the Fermi surface shown in Figure 1.4 by the solid arrow. Figure 1.4 is a cut of the Fermi surface (perpendicular to

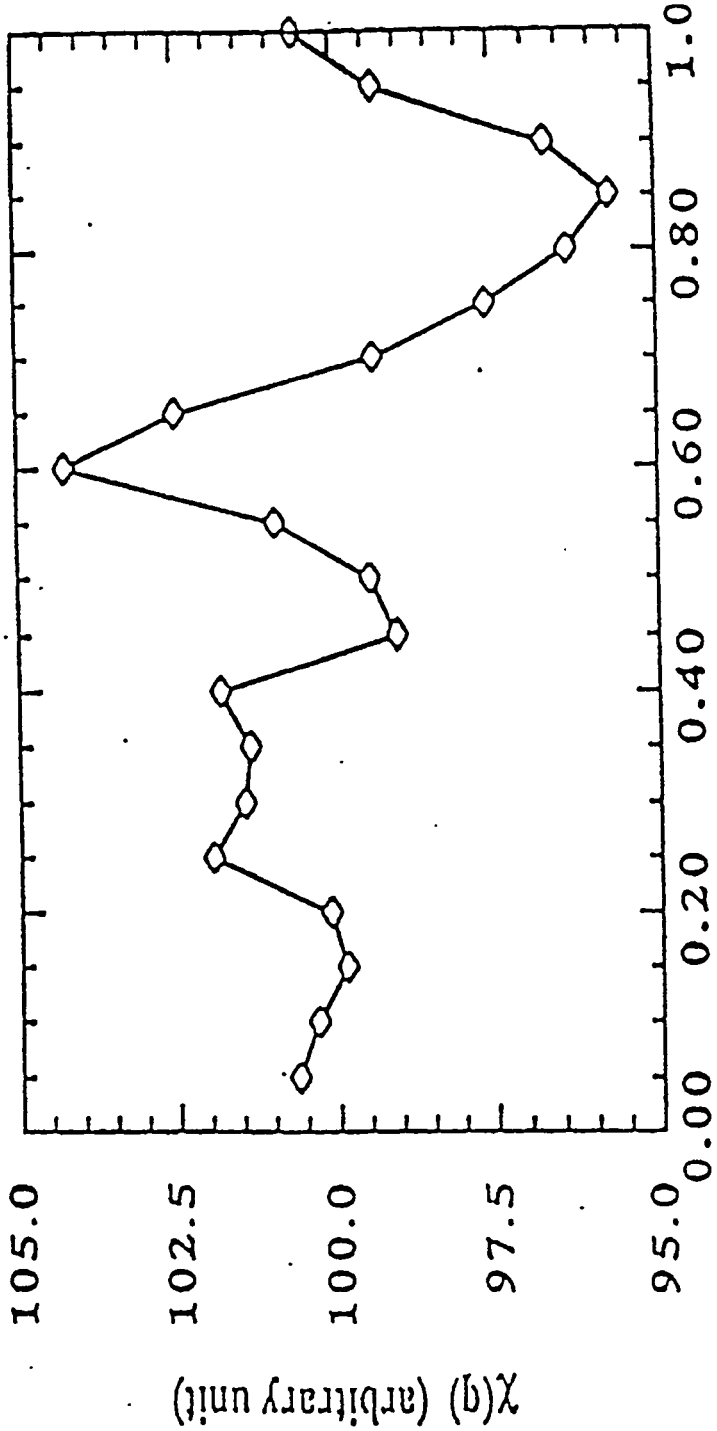

Figure 1.3: Generalized susceptibility along the a* axis. (After Reference Rhee[44])

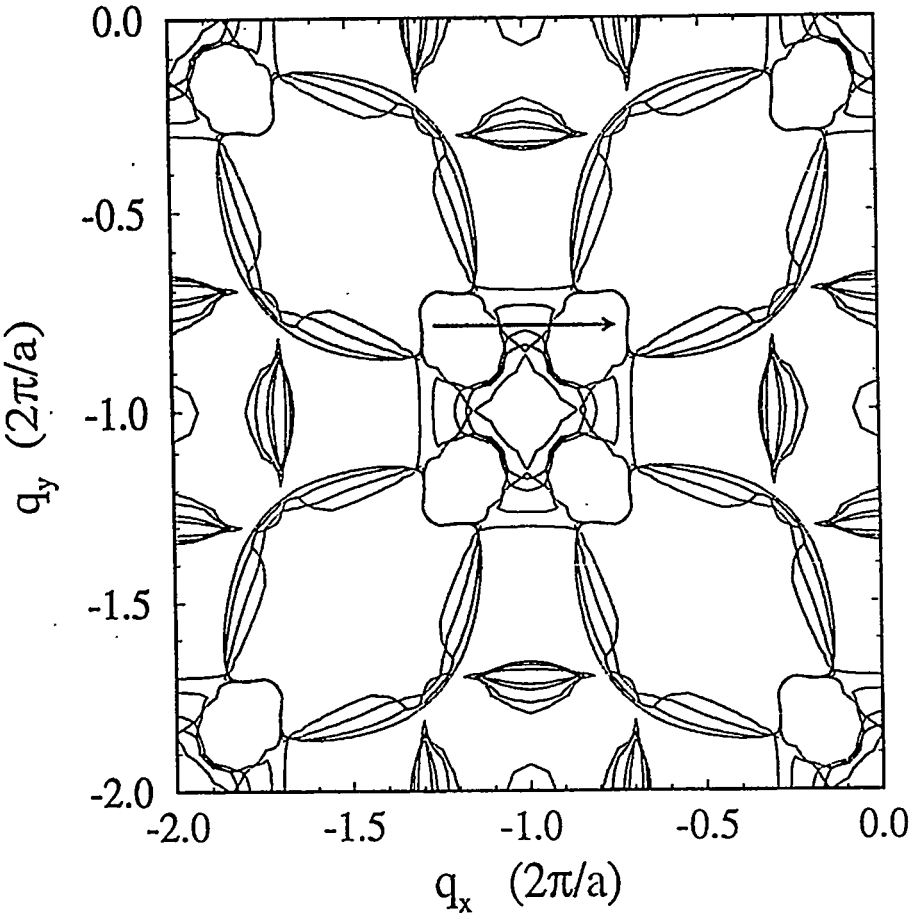

Figure 1.4: Fermi surface cross section on the planes perpendicular to the c axis. (After Reference Rhee[44])

the c axis) and the arrow shows the region of the Fermi surface that are nearly parallel and give rise to the peak in the generalized susceptibility $\chi(q)$ defined[45] as

$$\chi(\mathbf{q}) = \sum_{n,m,\mathbf{k}} \frac{f[E_m(\mathbf{k})]\{1 - f[E_n(\mathbf{k}+\mathbf{q})]\}}{E_n(\mathbf{k}+\mathbf{q}) - E_m(\mathbf{k})}$$

where f is the Fermi-Dirac distribution function and n, m are indexes of the electronic bands. Since there appears to be a strong nesting of the Fermi surface of $LuNi_2B_2C$[44], one would also expect strong Kohn anomalies in the phonon dispersion curves of this compound. This dissertation will detail the dispersion curves and Kohn anomalies in the Lu compound.

Other compounds in this family have been studied experimentally by other groups. Gompf et al.[46] found that the phonon softening in the $LuNi_2B_2C$ compound was so significant that it was observed in their phonon-density of states measurements. Likewise, Yanson et al.[47] found phonon softening in their point-contact spectra of these compounds. Kawano et al.[48] performed a detailed study of the low-lying excitations in the YNi_2B_2C compound and found softening as predicted above and claims that there may be a new type of excitations below the superconducting transition temperature.

Crystal Structure

The structure of these compounds[18] is body-centered tetragonal (space group I4/mmm) and consists of RE-C layers separated by Ni_2B_2 sheets as can be seen in Figure 1.1. The crystals used in these experiments were grown at the Ames Laboratory by the high-temperature flux technique.[49,50] With the high-temperature flux technique, crystals as large of 700 mg(7mm x 7mm x 0.5mm) can be grown. Typically the c-axis is around 3 times larger than the a-axis. Some typical lattice constants from neutron scattering experiments are given in Table 1.2.

Experimental-Neutron Scattering

This section will detail some practical aspects of neutron scattering directly related to this dissertation. Other texts cover the subject of neutron scattering[51,52,53,54,55,56] in much greater depth than this dissertation.

Unlike X-rays and electromagnetic radiation such as infrared radiation, neutrons have wavelengths and energies comparable with the interatomic spacing and phonon energies of solids. Taking this into account as well as the fact that neutrons have no electric charge, makes neutron

Table 1.2: Lattice constants from neutron scattering for $RENi_2B_2C$ (After Reference Siegrist[18]).

RE	Lat. Par. (a) Å	Lat. Par. (c) Å
Lu	3.467	10.63
Tm	3.494	10.6
Er	3.508	10.57
Ho	3.526	10.54
Dy	3.535	10.55
Y	3.544	10.47
Tb	3.561	10.43
Sm	3.629	10.23
La	3.803	9.795

scattering an ideal tool for the study of dynamical properties of crystalline solids. The neutron interacts with the nucleus primarily though the nuclear force. The range of the neutron-nucleon interaction is of the order of 1 Fermi while the wavelength of the incident neutrons is roughly 1 Å. This implies that neutron scattering is isotropic and can be characterized by a single parameter b, the scattering length. The value of b can be both positive, negative, or even complex depending on the nucleus involved. In addition, different isotopes and spin orientations of the neutron and nucleus also affect the scattering length.

Most crystals are made up of a variety of isotopes, and therefore b may vary from nucleus to nucleus. Only the mean scattering potential can give interference effects and thus have coherent scattering. Likewise, the variations in scattering potential from different nucleus is proportional to $(\overline{b^2}-\overline{b}^2)^{\frac{1}{2}}$ and give rise to incoherent scattering. The differential cross section for scattering of neutrons into the solid angle Ω can thus be represented as a sum of two terms:

$$\left(\frac{d\sigma}{d\Omega}\right)_{total}=\left(\frac{d\sigma}{d\Omega}\right)_{coherent}+\left(\frac{d\sigma}{d\Omega}\right)_{incoherent}$$

The differential cross section of one-phonon inelastic coherent scattering is given by

$$\left(\frac{\partial^2\sigma}{\partial\Omega\partial E_f}\right)_{coherent} = \frac{4\pi^3\hbar}{V_0}\frac{k_f}{k_i}\sum_{\vec{\tau},j,\vec{q}}\frac{(n+\frac{1}{2}\pm\frac{1}{2})}{\omega_j(\vec{q})}\left|F_j(\vec{Q})\right|^2_{coh}\delta(\hbar\omega\mp\hbar\omega_j(\vec{q}))\delta(\vec{Q}-(\vec{q}+\vec{\tau}))$$

where

V_0 is the volume of the primitive cell,

n = average occupation number = $n_{j\vec{q}} = \dfrac{1}{\exp[\frac{\hbar\omega_j(\vec{q})}{k_B T}]-1}$,

$\vec{q}$ = phonon wave vector,

$\hbar\omega_j(\vec{q})$ = energy of the phonon in the j^{th} mode with wave vector $\vec{q}$,

$\vec{\tau}$ = reciprocal lattice vector,

$\vec{Q}=\vec{k}_i-\vec{k}_f$ is the scattering vector,

$\hbar\omega=\dfrac{\hbar^2\left(k_i^2-k_f^2\right)}{2M_n}$ is the energy change of the neutron,

$\left|F_j(\vec{Q})\right|^2_{coh}=\left|\sum_k \bar{b}_k[\vec{Q}\cdot\vec{e}(k\mid j\vec{q})]e^{i\vec{Q}\cdot\vec{r}(k)}\dfrac{e^{-W_k}}{\sqrt{M_k}}\right|^2$ is the inelastic structure factor,

$\bar{b}_k=\dfrac{1}{N_k}\sum_k b_k$ is the coherent nuclear scattering amplitude of atom k,

N_k = number of atoms of type k in the crystal,

$\vec{r}(k)$ = the position vector of atom k with respect to the origin of the unit cell,

and W_k = Debye-Waller factor for atom k.

The delta functions in the differential cross section requires conservation of energy and momentum up to a reciprocal lattice vector. The ± signs indicate the creation(upper) and annihilation(lower) of a phonon in mode j with wave vector $\vec{q}$. Since the average occupation number goes to 0 at low temperatures, most phonon low temperature experiments have to be done with the creation of phonons, or energy loss to the neutrons so that $\left(n+\frac{1}{2}\pm\frac{1}{2}\right)$ is equal to 1, and not 0 at low temperatures.

Experimentally, we want to maximize the coherent scattering so that we can observe the phonon peaks and hopefully minimize the background. By looking at the inelastic structure factor, we see that it contains the following expression $\vec{Q}\cdot\vec{e}(k,j\vec{q})$. By maximizing $\vec{Q}$ we will be increasing the inelastic structure factor. This same expression is what determines which phonon polarization, or mode, will be picked up in a certain configuration. If the phonon polarization is parallel to $\vec{Q}$ the phonon mode should be observed in a scan. The $RENi_2B_2C$ phonon modes do not have the typical longitudinal and transverse symmetry along the [100] as are observed in most simple systems. Instead, these modes develop both transverse(along **c***) and longitudinal components for the Ni and B atoms for two of the four representations. The RE and C atoms on the other had, do not

exhibit both transverse and longitudinal components. For example, for small wave vectors, the Δ_4 is transverse in nature, however, as the wave vector increases, the Ni and B atoms develop a longitudinal component. This means that it is theoretically possible to pick this mode up from a longitudinal configuration. Only a complete analysis of the inelastic structure factors will tell you which Q will give you the largest structure factor.

The incoherent scattering cross section does not depend on $\vec{Q}$ and will be treated as background for these experiments. Typically, phonons will have a peak height of a few hundred counts with a background of 50 or less. Figures 1.5 and 1.6 show two phonon profiles for $LuNi_2B_2C$ and YNi_2B_2C respectively.

Experimental-Triple Axis Spectrometers

A schematic diagram of HB3 triple axis spectrometer at Oak Ridge National Laboratory(ORNL) is shown in Fig. 1.7. A large single crystal (pyrolitic graphite for these experiments) is used as a monochromator to Bragg reflect neutrons of a particular wavelength from the reactor spectrum. By varying the angle of the monochromator $2\theta_m$, and θ_m, the wavelength of the monochromatic beam can be varied.

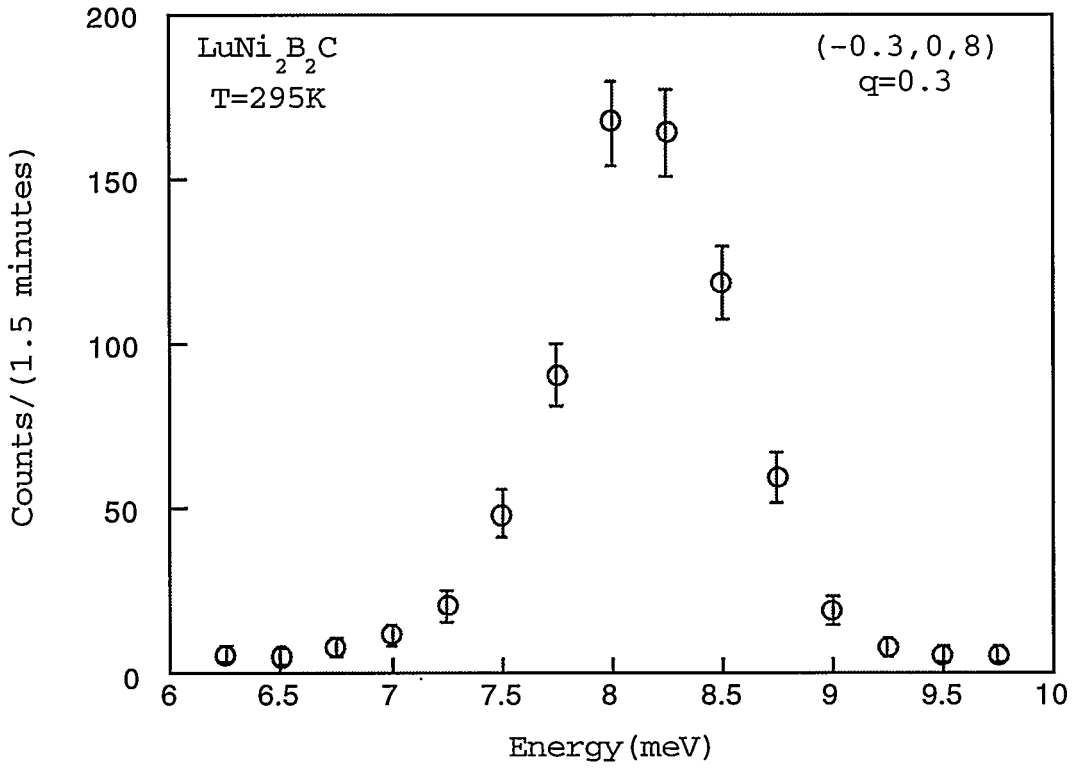

Figure 1.5: Phonon profile of $LUNi_2B_2C$ for Q=(0.3,0,8) at T=300K.

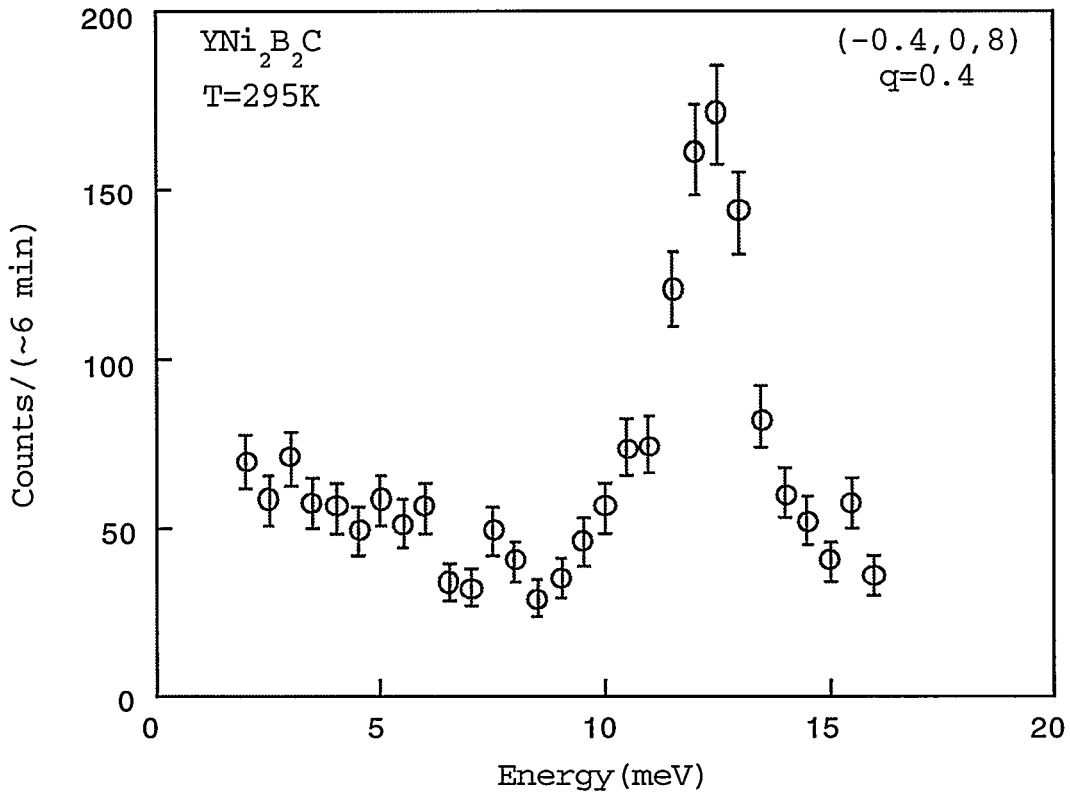

Figure 1.6: Phonon profile of YNi_2B_2C for Q=(0.3,0,8) at T=300K.

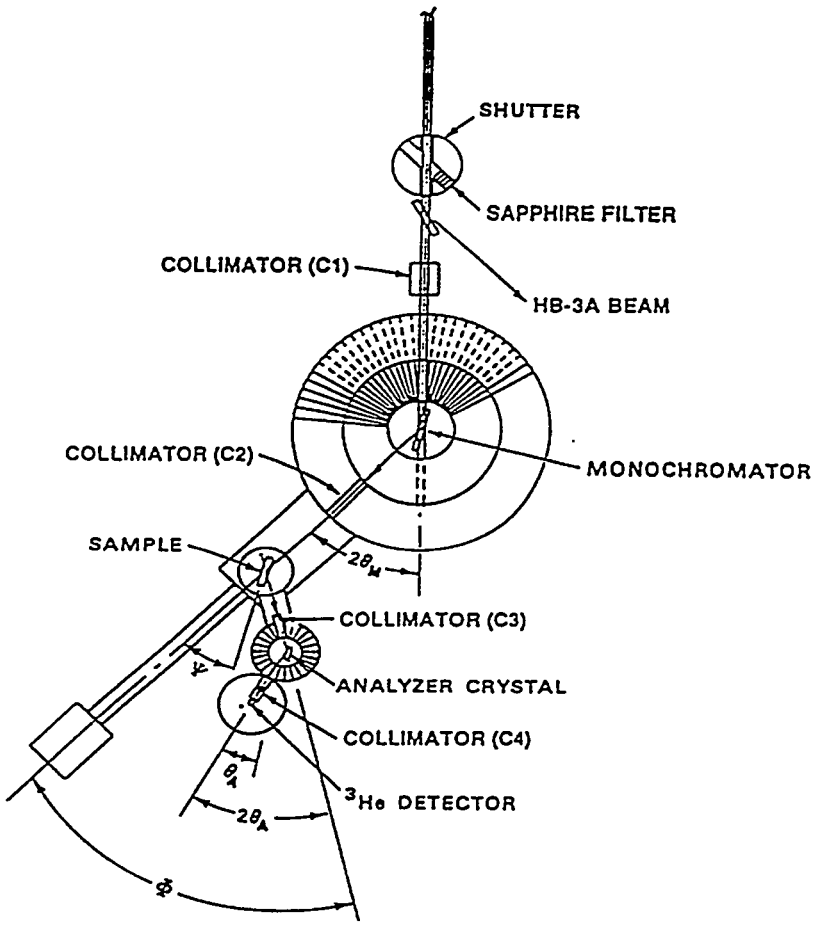

Figure 1.7: Diagram of the HB3 triple axis spectrometer at the HFIR reactor at Oak Ridge National Lab.

The momentum $\vec{k}_0$ of the incident neutrons of energy E_o is determined by the direction of the beam and the relation

$$E_0 = \frac{\hbar^2 k_0^2}{2M_n} = \frac{\hbar^2}{2M_n}\left[\frac{\pi \sin\theta_m}{d_m}\right],$$

where M_n is the mass of the neutron and d_m is the spacing of the reflecting planes of the monochromating crystal.

Next, the beam is incident on the sample crystal set at an angle ψ and is scattered at a scattering angle ϕ towards the analyzing crystal. The energy of the reflected beam of scattered neutrons is determined with the analyzer crystal. The final momentum of the neutrons is determined from the angle ϕ and the relation

$$E_f = \frac{\hbar^2 k_0^2}{2M_n} = \frac{\hbar^2}{2M_n}\left[\frac{\pi \sin\theta_a}{d_a}\right]$$

where θ_a is the glancing angle at the analyzer and d_a is the spacing of the reflecting planes of the analyzer.

Most of the experiments described in this dissertation were done at fixed analyzer energy of 14.5 meV, or 30.5 meV. These energies were chosen so that the pyrolitic graphite filters placed in front of the analyzer would attenuate higher-order contamination.

After the analyzer, the neutron beam travels into a detector. Since the neutron does not have any electric charge, a BF_3 or ^3He gas detector is typically used. The

neutron then interacts with the gas producing radiation by the relation

$$^{3}_{2}He + ^{1}_{0}n = ^{1}_{1}H + ^{3}_{1}H + 0.76\ Mev$$

Counters are typically cylindrical with a diameter of a few centimeters and a length of around 30 cm. These detectors have an efficiency of about 80%.

A typical spectrometer also has collimators along the path of neutrons to improve resolution of the instrument. Typically we use collimation of 40'-monochromator-40'-sample-40'-analyzer-80'-detector. Of course tighter collimation gives less background, but typically requires longer counting time to get the same intensity of the phonon peak. In addition, a sapphire filter was used before the monochromator in some experiments to eliminate higher energy neutrons.

Experimental-"Constant-Q" Method

The most common method used in determining the phonon dispersion relations using a triple axis spectrometer is the constant-Q method. In this method the scattering vector $\vec{Q} = \vec{k}_i - \vec{k}_f$ is held constant, while the energy transfer,

$$\hbar\omega = \frac{\hbar^2}{2M_n}\left(\vec{k}_i^{\,2} - \vec{k}_f^{\,2}\right)$$

is varied. This method is illustrated in Fig 1.8 and 1.9 for the (h01) scattering plane[we assume this plane is parallel

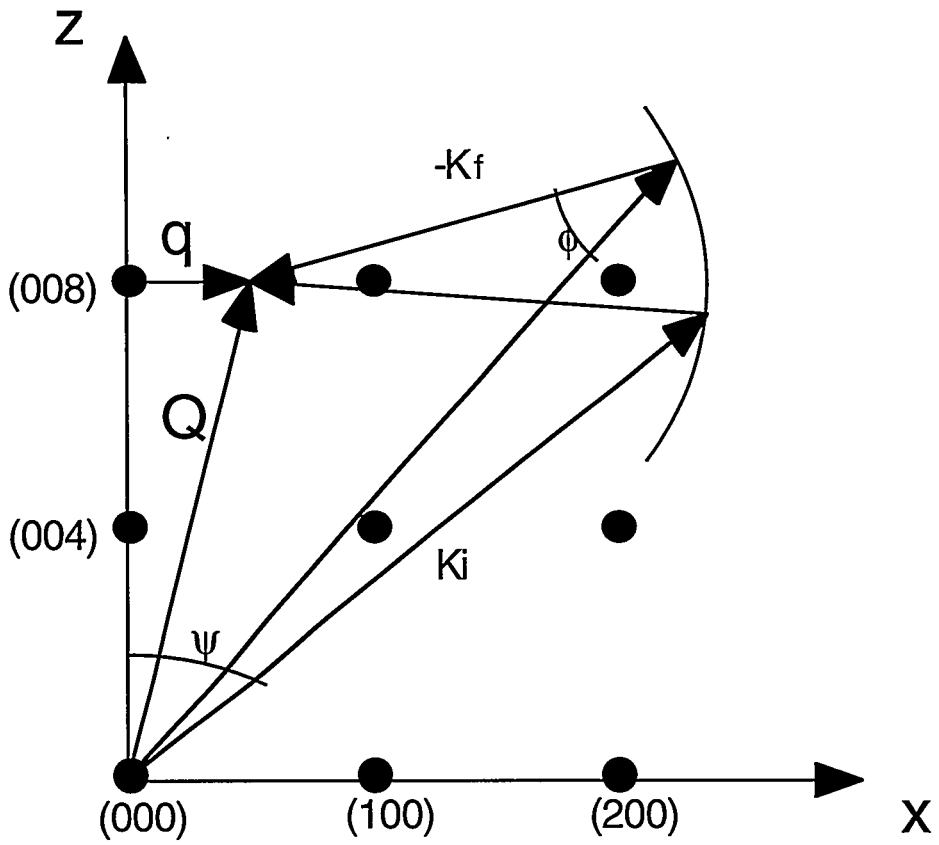

Figure 1.8: The constant Q method of phonon measurement. This figure illustrates the motion of momentum-space vectors in the (h0l) scattering plane for a constant Q scan using fixed final energy(i.e. fixed $|\vec{k}_f|$).

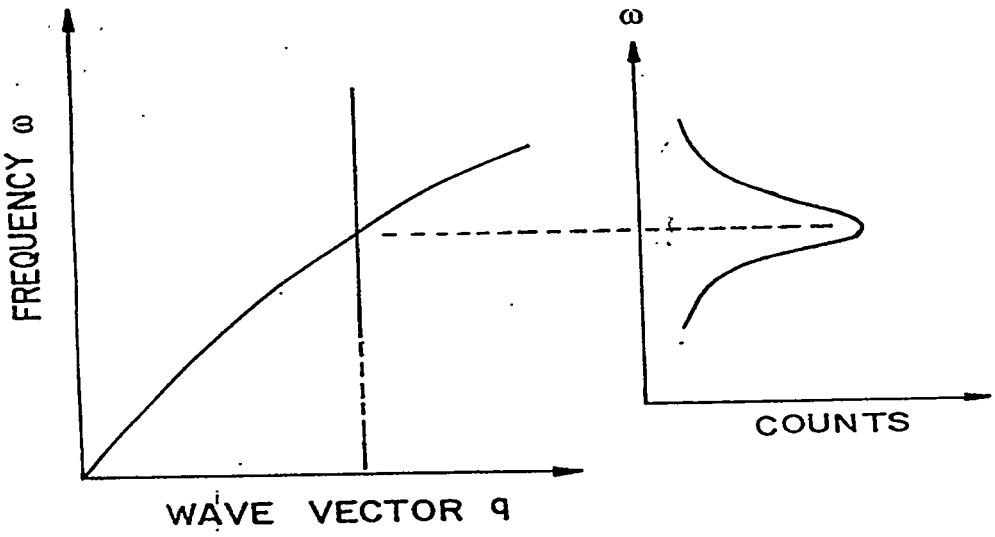

Figure 1.9: The constant Q method of phonon measurement. The left figure shows a scan through a dispersion curve as produced by this method, while the right figure shows the resultant scan we see experimentally.

to the scattering plane of the spectrometer]. This amounts to scanning along the solid line in Fig. 1.8. For these experiments, we usually fix the final energy, which in turn fixes the magnitude of $\vec{k}_f$. The magnitude and direction of $\vec{k}_i$ are then varied so that $\vec{Q}=\vec{k}_i-\vec{k}_f$ is held constant. This allows the energy transfer to be varied which results in a vertical scan through the dispersion curve as can be seen in the left side of Fig 1.9. This results in a peak of the 'neutron group' in the left side of Fig 1.9 which will define the frequency $\omega_j(\vec{q})$. By varying $\vec{q}$ we are then able to map out the dispersion curves for a sample. The different polarizations can be selected by using different $\vec{Q}$ which will favor certain modes and suppress others according to the inelastic structure factor discussed above. Usually only high symmetry directions are mapped out in this way. For this body-centered tetragonal, we have mapped some of the lower Δ, Λ, and Σ branches which are along the [100], [001] and [110] directions.

Dissertation Organization

The first chapter gives a brief overview of the system discussed in this dissertation. Chapters 2-5 and Appendix B of this dissertation consist of papers that are published, or have been submitted, which show experimental data regarding

the phonon softening of $LuNi_2B_2C$. The papers are in chronological order and show how the problem has progressed over time. Each of these papers has a list of references pertaining to that particular paper, which are located at the end of each chapter. The author's name is first on the last three papers, and second on the other two papers; the author played a significant role in the experimentation, data interpretation, and compiling of all five papers. At the t: is dissertation was completed, the paper that is cl 4 of this dissertation has not been approved by Pl l Review B for publication yet. In addition, the pa iven in appendix B is a rough draft of a proposed pa iat should be submitted shortly after the completion of dissertation.

Chapter 6 will contain a summary of the conclusions up to date. Appendix A will consist of a brief derivation of $\chi(q)$ which is talked about in the introduction of the dissertation. Appendix B will contain a Born-von Kármán model fit to the experimental $LuNi_2B_2C$ data and a comparison with experimental data. Appendix C will contain a brief summary of the work done on $LuNi_2B_2C$ as well as a complete listing of experimental data taken on the crystals which may be needed later for theoretical models of this system. Appendix D will outline a brief introduction covering some of the field theory used in the theoretical work for this

thesis. The bibliography at the end of the dissertation will contain references cited in Chapters 1, Chapter 6, and Appendices A, C, and D.

CHAPTER 6. CONCLUSION

In summary, the results obtained can be, at least, qualitatively understood both above as well as below T_c. For $T>T_c$, the softening of the two lowest Δ_4 branches can be understood in terms of two interacting modes. This is illustrated in Fig 6.1 where the results are compared with the model presented in the appendix of chapter 4[58].

For $T<T_c$, the experimental results clearly show that the origin of the dramatic change in the phonon spectra is the onset of superconductivity in these compounds. One of the direct effects of the superconducting gap opening is well understood and has been observed many years ago in superconducting Nb and Nb_3Sn[59,60]. A phonon with energy lower than the superconducting gap 2Δ cannot decay by breaking Cooper pairs and therefore its lifetime is increased (line width narrowing) compared to its lifetime above T_c. In addition, because of the singularity at $\omega \approx 2\Delta$ in the polarizability of the superconducting electrons, there is a shift in the phonon frequencies as well as a change in the phonon spectra as the temperature is decreased below T_c. Recent calculations of this change in phonon spectra by Allen et al.,[69] based on work by Schuster[71] and Zeyher et al.,[72] yield phonon spectra almost identical to those observed in this

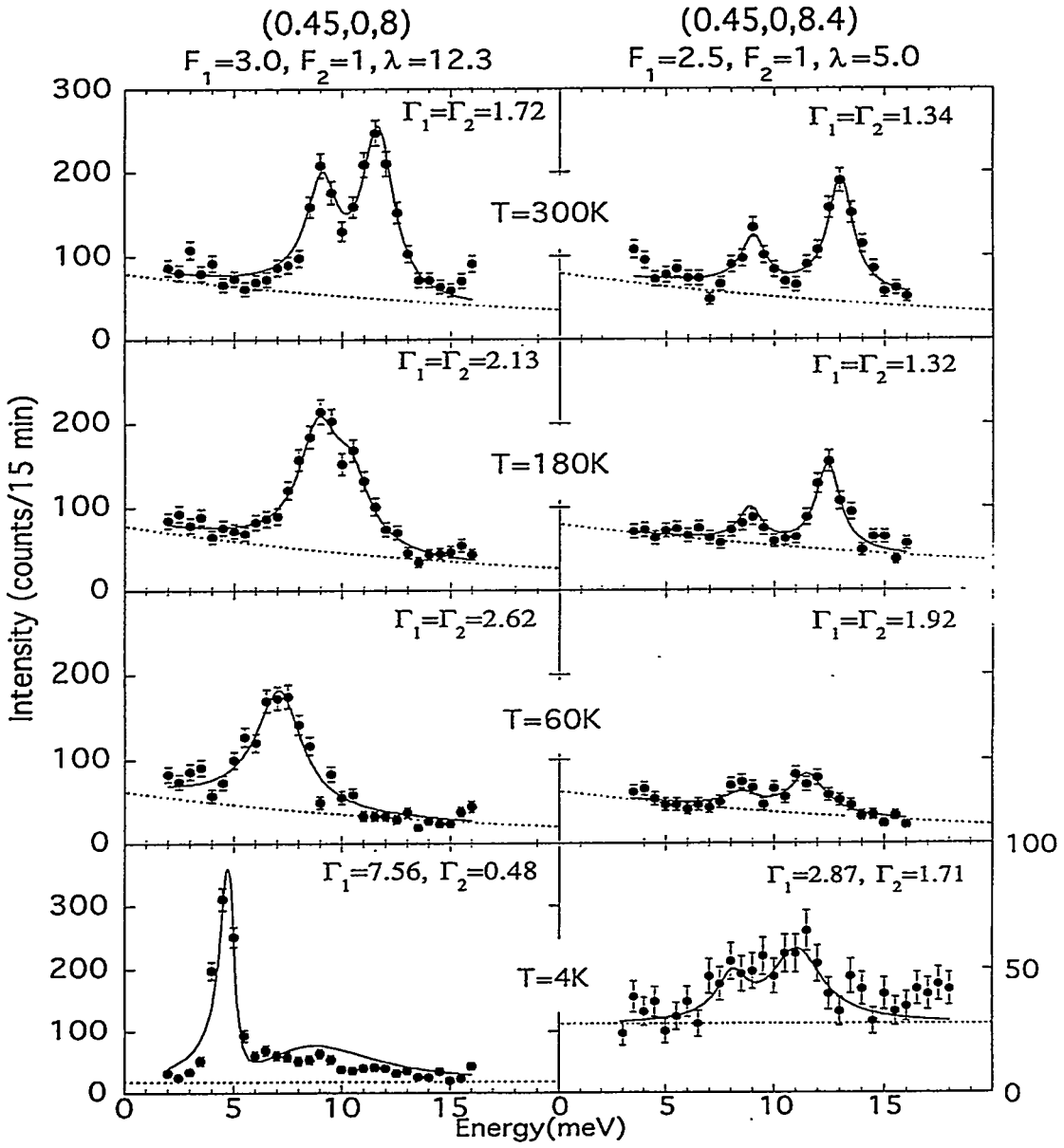

Fig. 6.1: Measured and calculated phonon profiles for several temperatures for (a) **Q**=(0.45,0,8) and (b) **Q**=(0.45,0,8.4). The calculations are based on the coupled-mode model described in the appendix of chapter 4.

dissertation. These calculations can be seen in Fig. 6.2. By looking at the right hand side, the observed spectra with instrumental resolution taken into account, we see that the spectra are very similar to the experimental phonon spectra observed at low T.

The above calculations are independent of q. Whereas in our case, the sharp feature is seen near a region that is known to have Fermi surface nesting. This suggests that these effects may be observable only when there is nesting. Kee and Varma[70] found that the electronic polarizability for an extremum vector of the Fermi surface exhibits a pole for frequencies close to 2Δ. For a phonon with normal state frequency above 2Δ this leads to a delta function in the polarizability at ω slightly below 2Δ and a peak centered around the normal state phonon frequency. The spectra, (See Fig 6.3) when convoluted with the instrumental resolution, is similar to those observed below T_c in the present experiments. The frequency of the observed sharp peak, on the other hand, does not follow the BCS temperature dependence of the superconducting gap as the Kee-Varma theory predicts.

The difference between the Kee-Varma and Allen et al. theory is due to the approximation involved in the evaluation of the electronic polarizability. Numerical calculation of the polarizability may be necessary to elucidate the difference.

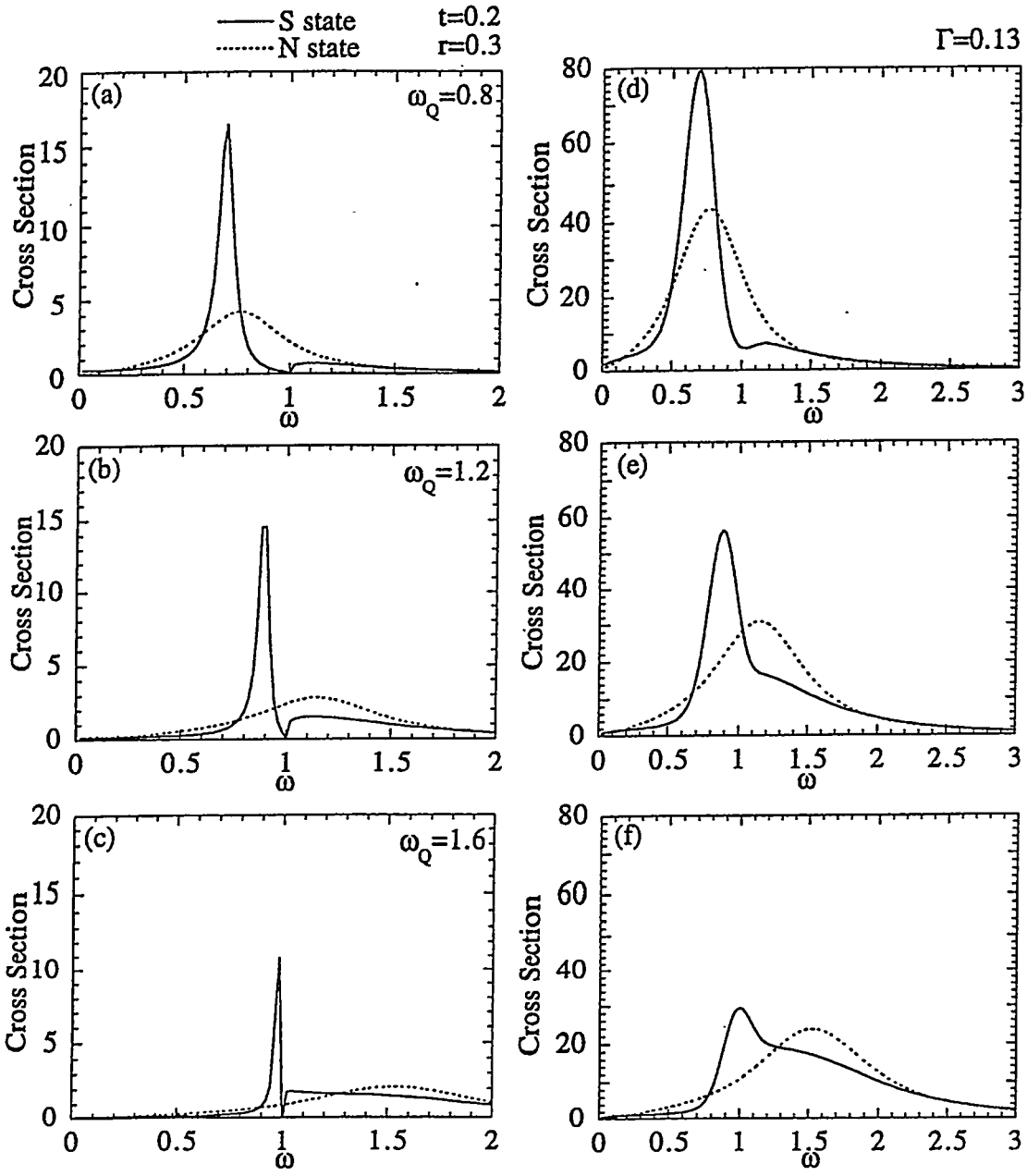

Fig. 6.2: Calculated line shapes at ω_Q=(a) 0.8, (b) 1.2, (c) 1.6 (units of 2Δ) at T/T_c=t=0.2. Panels (d)-(f) are convoluted with an instrumental broadening Γ=0.13 (units of 2Δ). (After reference Allen[69].)

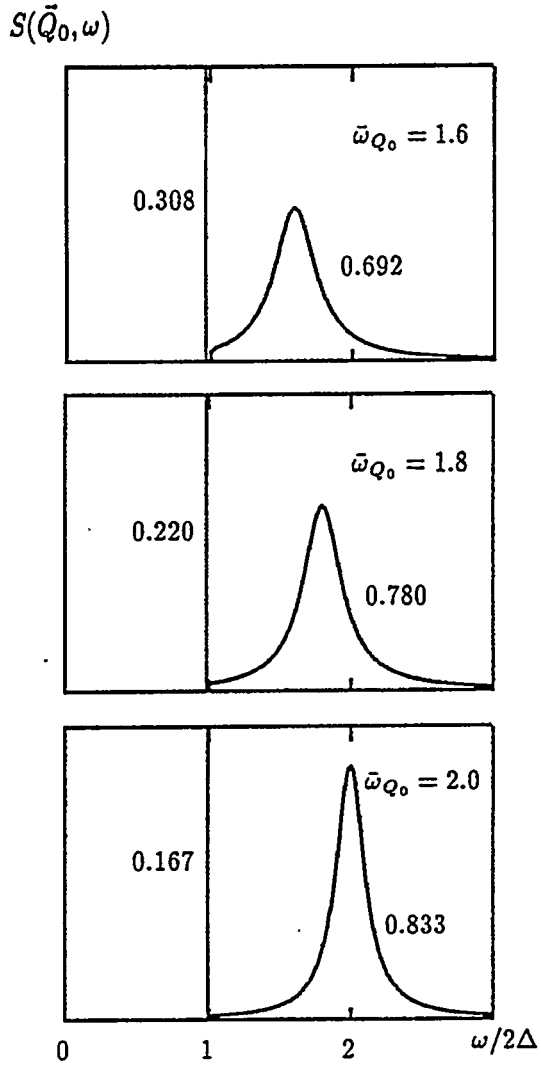

Fig. 6.3: Phonon spectral function $S(\mathbf{Q}_0,\omega)$ calculated for various ϖ_Q where $\varpi_Q = \omega_Q/2\Delta$, and $r=2\Delta=0.4N(0)$. (After reference Kee-Varma[70]).

Hopefully, other systems can be found that exhibit this sharp feature in the superconducting state so that this can be studied in greater detail. Since the characteristics of this sharp peak are determined by the superconducting properties of these systems, this work and future studies of these phonons may lead to the development of such measurements as a powerful technique for the study of the superconducting properties in these and other compounds.

APPENDIX A: DERIVATION OF $\chi(\mathbf{q})$

This appendix will follow the presentation of the electron-electron interaction given by Ziman.[73]

Electrons interact with other electrons via the Coulomb force. Usually we assume in materials that these interactions can be taken care of by assumptions that adjust the atomic potentials for the charge distribution of the valence electrons. Another option is to treat the gas of electons interacting via their Coulomb potential as a many-body problem. The basic effects of this interaction are now well understood.

To derive these results, we take a free-electron gas, subject to a time-dependent perturbation. Suppose that the potential seen by the elctron at r, at time t, is given by

$$\delta U(\mathbf{r},t) = Ue^{i\mathbf{q}\cdot\mathbf{r}}e^{i\omega t}e^{\alpha t}.$$

This perturbation is an oscillation, of frequency ω, wave-vector $\mathbf{q}$, that grows with a time-constant α. Perturbation acting on a state

$$|\mathbf{k}\rangle = e^{i\{\mathbf{k}\cdot\mathbf{r}+\frac{E(\mathbf{k})t}{\hbar}\}}$$

causes mixing of other states. This causes the wave-function to become

$$\psi_{\mathbf{k}}(\mathbf{r},t) = |\mathbf{k}\rangle + b_{\mathbf{k}+\mathbf{q}}(t)|\mathbf{k}+\mathbf{q}\rangle,$$

where the coefficients may be calculated, in first order, by perturbation theory;

$$b_{\mathbf{k+q}}(t) = \frac{\langle \mathbf{k+q} | \delta U | \mathbf{k} \rangle}{\mathrm{E}(\mathbf{k}) - \mathrm{E}(\mathbf{k+q}) + \hbar\omega - \mathrm{i}\hbar\alpha}$$

$$b_{\mathbf{k+q}}(t) = \frac{U e^{i\omega t} e^{\alpha t}}{\mathrm{E}(\mathbf{k}) - \mathrm{E}(\mathbf{k+q}) + \hbar\omega - \mathrm{i}\hbar\alpha} .$$

Now we will consider the change in charge density due to this change in the electron wave-functions. The electrons will see a uniform positively charged medium which will give the following change in charge denisty

$$\delta\rho(r,t) = e\sum_{\mathbf{k}} \{ \left| \psi_{\mathbf{k}}(\mathbf{r},t) \right|^2 - 1 \}$$

$$\delta\rho(r,t) = e\sum_{\mathbf{k}} [\{ e^{-i\mathbf{k}\cdot\mathbf{r}} + b^{*}_{\mathbf{k+q}}(t) e^{-i(\mathbf{k+q})\cdot\mathbf{r}} \} \{ e^{i\mathbf{k}\cdot\mathbf{r}} + b_{\mathbf{k+q}}(t) e^{i(\mathbf{k+q})\cdot\mathbf{r}} \} - 1] ,$$

or,

$$\delta\rho(r,t) \approx e\sum_{\mathbf{k}} \{ b_{\mathbf{k+q}}(t) e^{i\mathbf{q}\cdot\mathbf{r}} + b^{*}_{\mathbf{k+q}}(t) e^{-i\mathbf{q}\cdot\mathbf{r}} \} ,$$

if we drop the term in $|b|^2$. This summation is over all occupied electron states.

We see that there appears to be two types of wave traveling in opposite directions. Since the perturbation needs to be real, we can then add the complex conjugate to our origional perturbation, which tells us that the variation in charge density follows the total perturbation

$$\delta\rho = e\sum_{\mathbf{k}}\left\{\frac{\mathrm{U}}{\mathrm{E}(\mathbf{k})-\mathrm{E}(\mathbf{k}+\mathbf{q})+\hbar\omega-\mathrm{i}\hbar\alpha}+\frac{\mathrm{U}}{\mathrm{E}(\mathbf{k})-\mathrm{E}(\mathbf{k}+\mathbf{q})-\hbar\omega+\mathrm{i}\hbar\alpha}\right\}e^{i\mathbf{q}\cdot\mathbf{r}}e^{i\omega t}e^{\alpha t}+c.c$$

To further simplify this expression, let us introduce the Fermi-Dirac function, $f_0(\mathbf{k})$ as the probablility that $|\mathbf{k}\rangle$ is occupied in the unperturbed metal. Next, we will rewrite $\mathbf{k}$ for $\mathbf{k}$-$\mathbf{q}$ as labels in the second term, this leads to

$$\delta\rho(r,t) = eU\sum_{\mathbf{k}}\left\{\frac{\mathrm{f}_0(\mathbf{k})-f_0(\mathbf{k}+\mathbf{q})}{\mathrm{E}(\mathbf{k})-\mathrm{E}(\mathbf{k}+\mathbf{q})+\hbar\omega-\mathrm{i}\hbar\alpha}\right\}e^{i\mathbf{q}\cdot\mathbf{r}}e^{i\omega t}e^{\alpha t}+c.c$$

where the sum is over all states $|\mathbf{k}\rangle$.

By Poisson's equation

$$\nabla^2(\delta\phi) = -4\pi e\delta\rho$$

we see that the charge distribution gives rise to a potential-energy field acting on the electrons. If we assume that $\delta\phi$ has the same space and time variataion as $\delta\rho$, we can then write

$$\delta\phi(\mathbf{r},t) = \phi e^{i\mathbf{q}\cdot\mathbf{r}}e^{i\omega t}e^{\alpha t}+c.c\,.$$

Combining the last 3 equations, we end up with

$$-q^2\phi = -4\pi e^2U\sum_{\mathbf{k}}\left\{\frac{\mathrm{f}_0(\mathbf{k})-f_0(\mathbf{k}+\mathbf{q})}{\mathrm{E}(\mathbf{k})-\mathrm{E}(\mathbf{k}+\mathbf{q})+\hbar\omega-\mathrm{i}\hbar\alpha}\right\},$$

and by simplifing a little, we end up with

$$\phi = \frac{4\pi e^2}{q^2}\sum_{\mathbf{k}}\left\{\frac{\mathrm{f}_0(\mathbf{k})-f_0(\mathbf{k}+\mathbf{q})}{\mathrm{E}(\mathbf{k})-\mathrm{E}(\mathbf{k}+\mathbf{q})+\hbar\omega-\mathrm{i}\hbar\alpha}\right\}U\,.$$

This potential energy is associated with the charge redistribution created by the original potential δU. However, this new potential should have been counted as a perturbation of the electron distribution. To be consistant, we will assume that the perturbation δU already contains the term $\delta\phi$ given by

$$\delta U(\mathbf{r},t) = \delta V(\mathbf{r},t) + \delta\phi(\mathbf{r},t),$$

where $\delta V(\mathbf{r},t)$ is the external potential we applied at the start of the derivation. Combining all the expressions, we end up with

$$U = V + \left\{ \frac{4\pi e^2}{q^2} \sum_{\mathbf{k}} \frac{\mathrm{f}_0(\mathbf{k}) - f_0(\mathbf{k}+\mathbf{q})}{\mathrm{E}(\mathbf{k}) - \mathrm{E}(\mathbf{k}+\mathbf{q}) + \hbar\omega - \mathrm{i}\hbar\alpha} \right\} U$$

or

$$U = \frac{V}{\varepsilon(\mathbf{q},\omega)},$$

where

$$\varepsilon(\mathbf{q},\omega) = 1 + \left\{ \frac{4\pi e^2}{q^2} \sum_{\mathbf{k}} \frac{\mathrm{f}_0(\mathbf{k}) - f_0(\mathbf{k}+\mathbf{q})}{\mathrm{E}(\mathbf{k}+\mathbf{q}) - \mathrm{E}(\mathbf{k}) - \hbar\omega + \mathrm{i}\hbar\alpha} \right\}.$$

The effective potential U acting on the electrons is the applied potential V divided by the dielectric constant $\varepsilon(\mathbf{q},\omega)$. If we wish to examine screening effects for short distances, we need to look at large values of $\mathbf{q}$ and evaluate the summation. This will depend on the detailed structure of the energy surfaces $\mathrm{E}(\mathbf{k})$. For a free-electron model at absolute

zero it is not very difficult to evaluate the sum by a straightforward integration over **k**-space. This leads to the following expression

$$\varepsilon(\mathbf{q},0)=1+\frac{4\pi e^2}{q^2}\frac{n}{\frac{2}{3}E_f}\left\{\frac{1}{2}+\frac{4k_f^2-q^2}{8k_f q}\ln\left|\frac{2k_f+q}{2k_f-q}\right|\right\}$$

where k_f is the radius of the Fermi sphere. This result is interesting because at $2k_f$ the ln term is singular. This is the origin of the Kohn effect talked about in chapter 1. A phonon of wave-vector q sets up a potential with components like that for the dielectric function due to the motion of the ions. The electrons move to screen this field. This means that the ions now interact with one another via this screened field, which is inversely proportional to $\varepsilon(\mathbf{q})$. This means that the lattice frequencies will be modified depending on $\varepsilon(\mathbf{q})$. In other words, any singularity in $\varepsilon(\mathbf{q})$ will be reflected in the phonon frequency.

APPENDIX C: EXPERIMENTAL DATA FOR $LuNi_2B_2C$

The phonon dispersion curves for $LuNi_2B_2C$ were measured at the HFIR on the triple axis spectrometers HB1A, HB1, HB2, and HB3, and at the HFBR on the triple axis spectrometers H-7 and H-8. The dispersion curves were determined along the [100], [001], and [110] symmetry directions at varying temperatures from room temperature down to 1.8 K.

The typical experimental setup used for these scans are described in the introductory chapter of this thesis. To quickly summarize the experimental setup, most of the experimental data was obtained with phonon creation with a fixed final energy E_f equal to 14.7 meV. Some experiments were done at 30.5 meV also. Most of the experimental scan used constant Q, although some of the steeper dispersion curves were done in a constant energy configuration. Typically, we used collimation of 40'-monochromator-40'-sample-40'-analyzer-80'-detector, although tighter collimation was also used in some experiments. Most of the data collected at the HFIR was done with two crystal mounted together. For the low temperature experiments at HBRF, most of those experiments were done with only one single crystal.

The early work done on $LuNi_2B_2C$ was done at the HFIR reactor at Oak Ridge National Laboratory. This is where the

phonon softening of the two lowest Δ_4 branches was first observed, which resulted in our first paper which is chapter 2 of this thesis. After Kwano's paper on the YNi_2B_2C compound came out in *Physical Review Letters*, we then went back and studied the Lu compound in more detail. Those results are published in chapters 3-5 of this thesis. Most of this work was done in collaboration with Gen Shirane and Steve Shapiro of Brookhaven National Laboratory. These later experiments which looked exclusively at the phonon softening of the two lowest Δ_4 brances were done at BNL.

Table B.1 and B.2 contain a summary of most of the experimental phonon data collected on the $LuNi_2B_2C$ compound up to date. Table C.1 contains the temperature dependent data done at both the HFIR and HFRB for the two lowest Δ_4 branches. Table C.2 contains all other branches along the Δ direction as well as experimental data in the Λ and Σ directions. These tables differ from the experimental data in Appendix B in that this is a complete set of experimental data and the data in Appendix B is only the data used in the Born-von Kármán lattice dynamical calculations. The data in Appendix B are basically a summary of the room temperature data given in Tables C.1 and C.2.

Table C.1: Experimental data for the two Δ_1 branches that exhibit softening in $LuNi_2B_2C$.

Branch/q	Machine	Q	Date	T[K]	ω(meV)	Error
Δ_4						
0.10	HB3	(-0.1,0,8)	Apr-95	300	3.35	0.15
0.10	HB1A	(-0.1,0,8)	Mar-95	300	3.30	0.10
0.10	HB2	(0.1,0,8)	Feb-95	300	3.10	0.10
0.10	HB3	(-0.1,0,8)	Jun-95	300	3.32	0.10
0.20	HB3	(-0.2,0,8)	Apr-95	300	6.10	0.15
0.20	HB2	(0.2,0,8)	Feb-95	300	6.10	0.10
0.20	HB3	(-0.2,0,8)	Jun-95	300	6.00	0.10
0.20	HB3	(-0.2,0,8)	Apr-95	120	6.00	0.15
0.20	H8	(0.2,0,8)	Aug-96	15	5.50	0.20
0.20	H8	(0.2,0,8)	Aug-96	4	5.50	0.20
0.25	HB3	(-0.25,0,8)	Jun-95	2	6.90	0.10
0.30	HB3	(-0.3,0,8)	Apr-95	300	8.16	0.15
0.30	HB3	(0.3,0,8)	Feb-95	300	8.20	0.10
0.30	HB3	(-0.3,0,8)	Jun-95	300	8.10	0.15
0.30	HB3	(-0.3,0,8)	Apr-95	120	8.09	0.10
0.30	H8	(0.3,0,8)	Aug-96	15	7.50	0.20
0.30	HB3	(-0.3,0,8)	Apr-95	10	7.99	0.15
0.30	H8	(0.3,0,8)	Aug-96	4	7.50	0.20
0.30	HB3	(-0.3,0,8)	Jun-95	2	7.80	0.15
0.35	HB3	(-0.35,0,8)	Apr-95	120	8.60	0.20
0.35	H8	(-0.35,0,8)	Aug-96	30	8.00	0.40
0.35	H8	(-0.35,0,8)	Aug-96	15	8.00	0.30
0.35	H8	(-0.35,0,5)	Aug-96	4	7.70	0.20
0.36	H8	(-0.362,0,8)	Aug-96	15	8.00	0.40
0.36	H8	(-0.362,0,8)	Aug-96	4	8.00	0.30
0.38	H8	(-0.375,0,8)	Aug-96	75	8.00	0.40
0.38	H8	(-0.375,0,8)	Aug-96	30	8.00	0.40
0.38	H8	(-0.375,0,8)	Aug-96	15	5.00	0.40
0.38	H8	(-0.375,0,8)	Aug-96	4	5.50	0.30
0.38	H8	(-0.375,0,8)	Aug-96	4	7.50	0.50
0.40	HB2	(0.4,0,8)	Feb-95	300	9.60	0.20
0.40	HB3	(-0.4,0,8)	Jun-95	300	9.20	0.30
0.40	HB3	(-0.4,0,8)	Jun-95	300	9.15	0.20
0.40	HB3	(-0.4,0,8)	Jun-95	300	9.10	0.20
0.40	HB3	(-0.4,0,8)	Apr-95	120	8.49	0.25
0.40	HB3	(-0.4,0,8)	Jun-95	120	8.15	0.20
0.40	HB3	(-0.4,0,8)	Jun-95	60	7.60	0.20
0.40	HB3	(-0.4,0,8)	Aug-96	30	8.00	0.40
0.40	HB3	(-0.4,0,8)	Apr-95	25	7.70	0.25
0.40	HB3	(-0.4,0,8)	Jun-95	25	7.60	0.15
0.40	H8	(-0.4,0,8)	Aug-96	15	8.00	0.30

Table C.1 (continued)

0.40	HB3	(-0.4,0,8)	Apr-95	10	7.60	0.40
0.40	H8	(-0.4,0,8)	Aug-96	4	5.00	0.50
0.40	HB3	(-0.4,0,8)	Jun-95	2	7.50	0.20
0.41	HB3	(-0.41,0,8)	Apr-95	2	6.00	0.30
0.43	HB3	(-0.425,0,8)	Apr-95	120	8.43	0.20
0.43	HB3	(-0.425,0,8)	Apr-95	10	5.10	0.50
0.45	HB3	(-0.45,0,8)	Jun-95	300	8.90	0.50
0.45	HB3	(-0.45,0,8)	Jun-95	300	9.90	0.50
0.45	H8	(0.45,0,8)	Aug-95	75	8.00	0.50
0.45	HB3	(-0.45,0,8)	Jun-95	60	6.25	0.50
0.45	H8	(0.45,0,8)	Aug-95	30	6.00	0.50
0.45	HB3	(-0.45,0,8)	Jun-95	25	6.10	0.50
0.45	H8	(0.45,0,8)	Aug-95	15	6.00	0.30
0.45	HB3	(-0.45,0,8)	Jun-95	10	4.32	0.20
0.45	HB3	(-0.45,0,8)	Apr-95	10	4.20	0.40
0.45	H8	(0.45,0,8)	Aug-95	4	4.50	0.40
0.45	H8	(0.45,0,8)	Aug-96	4	5.00	0.50
0.45	HB3	(-0.45,0,8)	Jun-95	2	4.39	0.20
0.50	HB3	(0.5,0,8)	Jun-95	300	9.14	1.00
0.50	HB3	(-0.5,0,8)	Jun-95	300	9.50	1.00
0.50	HB3	(0.5,0,8)	Apr-95	120	8.74	0.30
0.50	HB3	(0.5,0,8)	Apr-95	120	8.70	0.50
0.50	H8	(0.5,0,8)	Aug-96	75	8.00	0.50
0.50	HB3	(0.5,0,8)	Apr-95	60	6.74	0.60
0.50	HB3	(-0.5,0,8)	Apr-95	60	7.74	0.40
0.50	H8	(0.5,0,8)	Aug-96	30	4.00	0.50
0.50	HB3	(0.5,0,8)	Apr-95	25	6.26	0.50
0.50	HB3	(-0.5,0,8)	Apr-95	25	6.52	0.60
0.50	HB3	(0.5,0,8)	Apr-95	10	3.80	0.50
0.50	HB3	(-0.5,0,8)	Apr-95	10	4.80	0.40
0.50	H8	(0.5,0,8)	Aug-96	4	4.00	0.40
0.50	HB3	(-0.5,0,8)	Jun-95	2	4.60	0.20
0.53	HB3	(-0.525,0,8)	Apr-95	10	6.00	0.30
0.55	HB3	(-0.55,0,8)	Jun-95	300	8.50	0.50
0.55	HB3	(-0.55,0,8)	Jun-95	300	8.60	0.50
0.55	HB3	(0.55,0,8)	Jun-95	300	8.70	0.50
0.55	HB3	(0.55,0,8)	Apr-95	10	5.76	0.40
0.55	H8	(0.55,0,8)	Aug-96	4	5.50	0.40
0.55	HB3	(-0.55,0,8)	Jun-95	2	6.00	0.20
0.60	HB3	(0.6,0,8)	Apr-95	120	8.59	0.15
0.60	HB3	(-0.6,0,8)	Apr-95	10	7.20	0.50
0.60	HB3	(-0.6,0,8)	Jun-95	2	7.00	0.50
0.70	HB3	(0.7,0,8)	Apr-95	300	8.75	0.30
0.70	HB2	(-0.7,0,8)	Feb-95	300	7.70	0.40

Table C.1 (Continued)

0.70	HB3	(0.7,0,8)	Apr-95	120	7.90	0.50
0.70	HB3	(0.7,0,8)	Apr-95	10	8.20	0.60
0.70	HB3	(0.7,0,8)	Jun-95	2	8.00	0.50
0.80	HB3	(0.8,0,8)	Apr-95	300	8.20	0.35
0.80	HB1A	(0.8,0,8)	Mar-95	300	8.00	0.60
0.80	HB2	(-0.8,0,8)	Feb-95	300	8.30	0.30
0.80	HB3	(0.8,0,8)	Apr-95	120	7.90	0.50
0.80	HB3	(0.8,0,8)	Apr-95	10	7.73	0.30
0.80	HB3	(0.8,0,8)	Jun-95	2	7.50	0.50
0.90	HB3	(0.9,0,8)	Apr-95	300	8.00	0.30
0.90	HB1A	(0.9,0,8)	Mar-95	300	8.00	0.70
0.90	HB2	(-0.9,0,8)	Feb-95	300	8.00	1.00
0.90	HB3	(0.9,0,8)	Apr-95	120	8.02	0.30
0.90	HB3	(0.9,0,8)	Apr-95	10	7.17	0.30
0.90	HB3	(0.9,0,8)	Jun-95	2	7.50	0.50
0.95	HB1A	(0.95,0,8)	Mar-95	300	7.45	0.15
0.95	HB3	(0.95,0,8)	Jun-95	2	7.00	0.30
1.00	HB3	(1,0,8)	Apr-95	300	8.34	0.30
1.00	HB1A	(1,0,8)	Mar-95	300	8.00	0.70
1.00	HB2	(-1,0,8)	Feb-95	300	8.30	0.30
1.00	HB2	(-1,0,10)	Feb-95	300	8.10	0.30
1.00	HB3	(1,0,8)	Apr-95	10	6.93	0.30
1.00	HB3	(1,0,8)	Jun-95	2	6.66	0.60
Δ_4 #2						
0.00	HB3	(0,0,8)	Apr-95	300	15.19	0.15
0.00	HB3	(1,0,7)	Apr-95	300	15.09	0.30
0.00	HB2	(1,0,7)	Feb-95	300	15.60	0.40
0.10	HB2	(0.9,0,7)	Feb-95	300	15.10	0.30
0.15	HB3	(0.15,0,8)	Apr-95	300	14.87	0.15
0.20	HB2	(0.8,0,7)	Feb-95	300	14.50	0.20
0.25	HB3	(0.25,0,8)	Apr-95	300	14.18	0.20
0.25	HB3	(0.25,0,8)	Jun-95	300	14.22	0.20
0.25	HB3	(0.25,0,8)	Apr-95	120	14.06	0.20
0.25	HB3	(0.25,0,8)	Apr-95	10	13.94	0.20
0.25	HB3	(0.25,0,8)	Jun-95	2	13.80	0.20
0.30	HB3	(0.3,0,8)	Jun-95	2	13.10	0.15
0.35	HB3	(0.35,0,8)	Apr-95	300	12.80	0.20
0.35	HB2	(0.65,0,7)	Feb-95	300	12.70	0.20
0.35	HB3	(0.35,0,8)	Jun-95	300	12.70	0.20
0.35	HB3	(0.35,0,8)	Apr-95	120	12.33	0.25
0.40	HB2	(-0.4,0,10)	Feb-95	300	11.40	0.40
0.40	HB3	(0.4,0,8)	Jun-95	300	11.85	0.20
0.40	HB3	(-0.4,0,8)	Jun-95	300	11.50	0.30
0.40	HB3	(0.4,0,8)	Apr-95	120	11.08	0.30

Table C.1 (Continued)

0.40	HB3	(0.4,0,8)	Jun-95	120	10.75	0.20
0.40	HB3	(0.4,0,8)	Jun-95	60	10.57	0.20
0.40	HB3	(0.4,0,8)	Apr-95	25	10.50	0.30
0.40	HB3	(0.4,0,8)	Jun-95	25	10.44	0.20
0.40	HB3	(0.4,0,8)	Apr-95	10	10.40	0.30
0.40	HB3	(0.4,0,8)	Jun-95	2	10.80	0.30
0.45	HB3	(0.45,0,8)	Jun-95	300	11.15	0.25
0.45	HB3	(0.45,0,8)	Jun-95	300	11.73	0.30
0.45	HB3	(0.45,0,8)	Jun-95	300	11.23	0.30
0.45	HB3	(0.45,0,8)	Jun-95	60	9.60	1.00
0.45	HB3	(0.45,0,8)	Jun-95	25	9.00	1.00
0.45	HB3	(0.45,0,8)	Jun-95	10	8.70	1.50
0.45	HB3	(0.45,0,8)	Jun-95	2	8.50	1.00
0.46	HB3	(0.46,0,8)	Apr-95	120	11.00	0.50
0.50	HB3	(0.5,0,8)	Apr-95	300	11.73	0.25
0.50	HB3	(0.5,0,8)	Apr-95	300	11.53	0.30
0.50	HB3	(-0.5,0,8)	Apr-95	300	12.20	0.15
0.50	HB3	(-0.5,0,8)	Apr-95	300	12.00	0.30
0.50	HB1A	(-0.5,0,8)	Mar-95	300	11.85	0.20
0.50	HB2	(0.5,0,8)	Feb-95	300	12.40	0.20
0.50	HB3	(0.5,0,8)	Jun-95	300	11.38	0.30
0.50	HB3	(-0.5,0,8)	Jun-95	300	11.80	0.30
0.50	HB3	(-0.5,0,8)	Jun-95	300	11.85	0.30
0.50	HB3	(0.5,0,8)	Apr-95	120	9.50	0.50
0.50	HB3	(-0.5,0,8)	Apr-95	120	9.50	0.40
0.50	HB3	(-0.5,0,8)	Apr-95	120	9.24	0.40
0.50	HB3	(-0.5,0,8)	Apr-95	10	9.30	0.40
0.50	HB3	(-0.5,0,8)	Jun-95	2	8.90	1.00
0.55	HB3	(-0.55,0,8)	Jun-95	300	12.93	0.30
0.55	HB3	(-0.55,0,8)	Jun-95	300	13.14	0.30
0.55	HB3	(-0.55,0,8)	Jun-95	300	12.88	0.30
0.55	HB3	(0.55,0,8)	Jun-95	300	12.48	0.30
0.55	HB3	(-0.55,0,8)	Apr-95	10	8.45	0.50
0.55	HB3	(-0.55,0,8)	Jun-95	2	8.50	1.00
0.60	HB3	(-0.6,0,8)	Apr-95	300	14.22	0.25
0.60	HB1A	(-0.6,0,8)	Mar-95	300	14.13	0.25
0.60	HB1A	(-0.6,0,8)	Mar-95	300	14.50	0.80
0.60	HB2	(0.6,0,8)	Feb-95	300	14.10	0.40
0.60	HB3	(0.6,0,8)	Jun-95	300	13.30	0.40
0.60	HB3	(-0.6,0,8)	Apr-95	120	12.91	0.20
0.60	HB3	(-0.6,0,8)	Apr-95	10	10.30	0.50
0.60	HB3	(0.6,0,8)	Jun-95	2	11.50	1.00
0.65	HB3	(-0.65,0,8)	Apr-95	300	15.06	0.30
0.65	HB3	(0.65,0,8)	Jun-95	300	14.72	0.30

Table C.1 (Continued)

0.65	HB3	(-0.65,0,8)	Apr-95	120	13.88	0.30
0.65	HB3	(-0.65,0,8)	Apr-95	60	13.36	0.25
0.65	HB3	(-0.65,0,8)	Apr-95	25	13.23	0.30
0.65	HB3	(-0.65,0,8)	Apr-95	10	13.00	0.60
0.70	HB3	(-0.7,0,8)	Apr-95	300	15.38	0.20
0.70	HB3	(0.7,0,8)	Apr-95	300	15.21	0.25
0.70	HB2	(-0.7,0,8)	Feb-95	300	15.60	0.20
0.70	HB1A	(-0.7,0,8)	Mar-95	300	16.30	0.70
0.70	HB3	(0.7,0,8)	Apr-95	120	14.80	0.40
0.70	HB3	(-0.7,0,8)	Apr-95	10	14.00	0.30
0.70	HB3	(0.7,0,8)	Jun-95	2	14.00	0.70
0.75	HB1A	(0.75,0,8)	Mar-95	300	15.06	0.30
0.80	HB3	(0.8,0,8)	Apr-95	300	13.75	0.30
0.80	HB1A	(0.8,0,8)	Mar-95	300	14.00	1.00
0.80	HB2	(-0.8,0,8)	Feb-95	300	13.50	1.00
0.80	HB3	(0.8,0,8)	Jun-95	300	13.76	0.40
0.80	HB3	(0.8,0,8)	Apr-95	120	13.70	0.50
0.80	HB3	(0.8,0,8)	Apr-95	10	13.42	0.30
0.80	HB3	(0.8,0,8)	Jun-95	2	13.30	0.50
0.85	HB3	(0.85,0,8)	Jun-95	300	12.20	0.50
0.90	HB3	(0.9,0,8)	Jun-95	300	11.00	1.00

Table C.2: Experimental data for the other branches in $LuNi_2B_2C$

Branch/q	Machine	Q	Date	ω(meV)	Error
Δ_1					
0.05	HB3	(2.05,0,0)	Jun-95	4.00	0.20
0.11	HB2	(2.11,0,0)	Mar-95	7.50	0.20
0.15	HB3	(2.15,0,0)	Apr-95	9.75	0.30
0.15	HB3	(2.15,0,0)	Aug-95	9.54	0.20
0.15	HB3	(2.15,0,0)	Aug-95	9.90	0.20
0.15	HB1A	(2.15,0,0)	Aug-95	9.90	0.20
0.20	HB2	(2.195,0,0)	Feb-95	12.00	0.30
0.20	HB2	(2.2,0,0)	Feb-95	12.30	0.20
0.25	HB3	(2.25,0,0)	Jun-95	13.90	0.35
0.29	HB2	(2.294,0,0)	Feb-95	16.00	0.40
0.35	HB3	(2.35,0,0)	Apr-95	17.00	0.30
0.35	HB1A	(2.35,0,0)	Feb-95	17.40	0.40
0.35	HB3	(2.35,0,0)	Jun-95	17.00	0.50
0.35	HB3	(2.35,0,0)	Aug-95	16.80	0.40
0.40	HB2	(2.4,0,0)	Feb-95	18.50	0.50
0.40	HB3	(0.6,0,9)	Jun-95	17.70	0.35
0.50	HB3	(2.5,0,1)	Apr-95	19.30	0.50
0.60	HB3	(2.4,0,1)	Apr-95	17.60	0.30
0.60	HB3	(2.4,0,1)	Jun-95	17.70	0.30
0.65	HB1A	(2.35,0,1)	Mar-95	16.60	0.60
0.70	HB3	(2.3,0,1)	Apr-95	15.60	0.20
0.80	HB1A	(2.2,0,1)	Apr-95	13.40	0.15
0.85	HB3	(2.15,0,1)	Jun-95	11.84	0.30
0.90	HB3	(2.1,0,1)	Apr-95	10.50	0.15
0.90	HB1A	(2.1,0,1)	Mar-95	10.40	0.15
0.95	HB1A	(2.05,0,1)	Mar-95	9.60	0.15
1.00	HB3	(2,0,1)	Apr-95	9.42	0.15
Δ_1 #2					
0.05	HB1A	(2.05,0,0)	Mar-95	14.05	0.30
0.15	HB1A	(2.15,0,0)	Mar-95	16.60	0.25
0.20	HB1A	(2.2,0,0)	Mar-95	18.40	0.25
0.25	HB1A	(2.25,0,0)	Mar-95	20.40	0.50
0.25	HB3	(2.25,0,0)	Jun-95	20.60	0.50
0.30	HB1A	(2.3,0,0)	Mar-95	23.00	0.40
0.30	HB3	(0.7,0,9)	Jun-95	22.30	0.60
0.40	HB1A	(0.6,0,9)	Mar-95	22.00	0.40
0.40	HB3	(0.6,0,9)	Jun-95	22.40	0.30
0.40	HB3	(0.6,0,9)	Jun-95	22.40	0.50
0.50	HB3	(0.5,0,9)	Apr-95	23.46	0.50
0.50	HB1A	(0.5,0,9)	Mar-95	23.42	0.60
0.60	HB1A	(0.4,0,9)	Mar-95	23.70	0.50

Table C.2 (Continued)

0.70	HB1A	(0.3,0,9)	Mar-95	24.50	0.80
0.80	HB1A	(1.8,0,9)	Mar-95	25.50	1.00
0.80	HB1A	(0.2,0,9)	Mar-95	25.80	0.70
0.90	HB3	(0.1,0,9)	Apr-95	25.15	0.40
0.90	HB1A	(0.1,0,9)	Mar-95	26.00	0.40
1.00	HB1A	(0,0,9)	Mar-95	26.40	0.40
Δ_1 #3					
0.00	HB1A	(1,0,9)	Mar-95	23.60	0.60
0.00	HB3	(1,0,9)	Jun-95	23.40	0.30
0.10	HB3	(0.9,0,9)	Apr-95	23.54	0.30
0.20	HB1A	(0.8,0,9)	Mar-95	25.50	0.40
0.20	HB3	(0.8,0,9)	Jun-95	23.00	0.25
0.40	HB1A	(2.4,0,0)	Mar-95	27.10	0.50
0.50	HB3	(2.5,0,0)	Jun-95	30.50	0.60
0.50	HB1A	(2.5,0,0)	Mar-95	30.70	0.50
Δ_3					
0.10	HB3	(2,0.1,0)	Aug-95	4.94	0.15
0.15	HB3	(2,0.15,0	Aug-95	7.00	0.20
0.15	HB3	(2,0.15,0)	Aug-95	7.10	0.15
0.30	HB3	(2,0.3,0)	Aug-95	11.75	0.50
0.40	HB3	(2,0.4,0)	Aug-95	13.20	0.30
Δ_3 #2					
0.15	HB3	(2,0.15,0)	Aug-95	15.25	0.30
0.30	HB3	(2,0.3,0)	Aug-95	19.70	0.40
0.50	HB3	(2,0.5,0)	Aug-95	26.50	0.40
0.75	HB3	(4,0.75,0)	Aug-95	32.80	0.50
0.90	HB3	(4,0.9,0)	Aug-95	34.90	0.70
1.00	HB3	(4,1,0)	Aug-95	36.00	2.00
Δ_4 #2					
0.60	HB3	(0.6,0,10)	Jun-95	26.05	0.60
0.70	HB3	(0.7,0,10)	Jun-95	24.30	0.60
0.80	HB3	(0.8,0,10)	Jun-95	23.80	0.70
1.00	HB3	(1,0,10)	Jun-95	23.90	0.50
Λ_3					
0.20	HB3	(2,0,0.2)	Jun-95	2.23	0.10
0.20	HB3	(2,0,0.2)	Apr-95	2.26	0.15
0.20	HB2	(2,0,-0.2)	Feb-95	2.20	0.15
0.30	HB3	(2,0,0.3)	Apr-95	3.34	0.15
0.30	HB1A	(2,0,0.3)	Mar-95	3.21	0.15
0.30	HB2	(2,0,-0.3)	Feb-95	3.50	0.10
0.30	HB3	(2,0,0.3)	Jun-95	3.32	0.15
0.40	HB3	(2,0,0.4)	Jun-95	4.26	0.10
0.50	HB3	(2,0,0.5)	Apr-95	5.22	0.15

Table C.2 (Continued)

0.50	HB2	(2,0,-0.5)	Feb-95	5.50	0.10
0.60	HB3	(2,0,0.6)	Jun-95	6.07	0.15
0.70	HB2	(2,0,-0.7)	Feb-95	7.10	0.10
0.80	HB3	(2,0,0.8)	Apr-95	7.78	0.15
0.80	HB1A	(2,0,0.8)	Mar-95	7.76	0.15
0.90	HB2	(2,0,-0.9)	Feb-95	8.60	0.10
0.90	HB3	(2,0,0.9)	Apr-95	8.57	0.15
0.95	HB3	(2,0,0.95)	Apr-95	8.89	0.15
0.95	HB3	(2,0,0.95)	Jun-95	8.80	0.10
1.00	HB3	(2,0,1)	Apr-95	9.42	0.10
1.00	HB2	(2,0,-1)	Feb-95	9.40	0.10
Λ_3 #2					
0.00	HB3	(2,0,0)	Apr-95	13.88	0.20
0.00	HB3	(2,0,0)	Jun-95	13.88	0.20
0.05	HB3	(2,0,-0.05)	Apr-95	14.01	0.15
0.20	HB3	(2,0,-0.2)	Apr-95	13.77	0.15
0.20	HB2	(4,0,0.2)	Feb-95	13.70	0.50
0.40	HB3	(2,0,-0.4)	Apr-95	13.01	0.20
0.40	HB1A	(2,0,-0.4)	Mar-95	12.95	0.30
0.40	HB2	(4,0,0.4)	Feb-95	13.30	0.30
0.60	HB3	(2,0,-0.6)	Apr-95	12.17	0.20
0.60	HB2	(4,0,0.6)	Feb-95	12.10	0.30
0.60	HB1A	(2,0,-0.6)	Mar-95	12.00	0.25
0.70	HB2	(2,0,0.7)	Feb-95	11.30	0.40
0.80	HB3	(2,0,-0.8)	Apr-95	10.85	0.25
0.80	HB1A	(2,0,-0.8)	Mar-95	10.50	0.25
0.90	HB3	(2,0,-0.9)	Apr-95	10.10	0.20
0.90	HB1A	(2,0,-0.9)	Mar-95	10.00	0.70
Λ_1					
0.20	HB3	(0,0,8.2)	Jun-95	4.30	0.40
0.30	HB2	(0,0,8.3)	Feb-95	6.30	0.30
0.40	HB3	(0,0,8.4)	Apr-95	8.08	0.20
0.40	HB1A	(0,0,8.4)	Mar-95	8.07	0.15
0.40	HB2	(0,0,8.4)	Feb-95	7.80	0.40
0.50	HB2	(0,0,8.5)	Feb-95	8.40	0.30
0.60	HB3	(0,0,8.6)	Apr-95	8.80	0.25
0.60	HB2	(0,0,8.6)	Feb-95	8.90	0.30
0.70	HB2	(0,0,8.7)	Feb-95	9.00	0.30
0.70	HB3	(0,0,8.7)	Jun-95	8.92	0.25
0.80	HB3	(0,0,8.8)	Jun-95	8.21	0.20
0.80	HB2	(0,0,10.8)	Feb-95	7.70	0.50
0.90	HB3	(0,0,8.9)	Apr-95	8.39	0.15
0.90	HB2	(0,0,10.9)	Feb-95	8.90	0.30
0.95	HB3	(1,0,7.95)	Jun-95	8.23	0.25

Table C.2 (Continued)

1.00	HB3	(1,0,8)	Jun-95	8.24	0.15
Λ_1 #2					
0.00	HB3	(0,0,8)	Apr-95	15.19	0.15
0.10	HB3	(0,0,8.1)	Jun-95	15.00	0.25
0.20	HB3	(0,0,8.2)	Apr-95	15.38	0.20
0.20	HB3	(0,0,8.2)	Jun-95	16.04	0.15
0.30	HB1A	(0,0,8.3)	Mar-95	16.04	0.15
0.40	HB1A	(0,0,8.4)	Mar-95	17.10	0.15
0.50	HB1A	(0,0,8.5)	Mar-95	18.40	0.20
0.60	HB1A	(0,0,8.6)	Mar-95	20.10	0.30
0.70	HB1A	(0,0,8.7)	Mar-95	22.10	0.10
0.90	HB3	(0,0,8.9)	Apr-95	24.96	0.20
0.90	HB1A	(0,0,8.9)	Mar-95	24.80	0.25
1.00	HB1A	(0,0,9)	Mar-95	26.40	0.40
Λ_2					
0.00	HB3	(1,0,9)	Jun-95	23.40	0.30
0.20	HB3	(1,0,9.2)	Jun-95	23.40	0.30
0.40	HB3	(1,0,9.4)	Jun-95	23.70	0.30
0.70	HB3	(1,0,9.7)	Jun-95	23.80	0.30
0.80	HB3	(1,0,9.8)	Jun-95	24.10	0.35
1.00	HB3	(1,0,10)	Jun-95	23.80	0.40
Σ_1					
0.06	HB3	(2.06,.06,0)	Aug-95	6.00	0.30
0.10	HB3	(2.1,2.1,0)	Aug-95	9.80	0.40
0.15	HB3	(2.15,2.15,0)	Aug-95	15.50	0.50
0.40	HB3	(1.6,2.4,0)	Aug-95	18.40	1.00
Σ_1 #2					
0.00	HB3	(2,2,0)	Aug-95	13.80	0.30
0.10	HB3	(2.1,2.1,0)	Aug-95	17.00	0.30
0.20	HB3	(2.2,2.2,0)	Aug-95	24.60	0.40
0.30	HB3	(2.3,2.3,0)	Aug-95	32.00	0.60
0.50	HB3	(2.5,2.5,0)	Aug-95	36.00	1.50
Σ_3					
0.10	HB3	(2.1,0.1,0)	Aug-95	4.54	0.25
0.13	HB3	(2.13,0.13,0)	Aug-95	6.60	0.20
0.20	HB3	(2.2,.2,0)	Aug-95	8.70	0.20
0.25	HB3	(2.25,0.25,0)	Aug-95	10.60	0.30
0.30	HB3	(2.3,0.3,0)	Aug-95	12.50	0.30
0.40	HB3	(1.6,2.4,0)	Aug-95	15.00	0.40
0.40	HB3	(3.6,0.4,0)	Aug-95	15.00	0.60
0.45	HB3	(2.45,0.45,0)	Aug-95	15.70	0.30
0.50	HB3	(1.5,2.5,0)	Aug-95	16.80	0.60
0.50	HB3	(1.5,2.5,0)	Aug-95	16.90	0.40

Table C.2 (Continued)

Σ_3 #2					
0.10	HB3	(1.9,2.1,0)	Aug-95	14.00	0.50
0.25	HB3	(1.75,2.25,0)	Aug-95	16.10	0.60

APPENDIX D. DYSON'S EQUATION

This appendix will follow the derivation given by Mattuck.[74]

Before we get to Dyson's equation, we will talk briefly about Green's function propagators. The Green's function propagator is usually in the form

$$G(k_2,k_1,t_2-t_1)=-i\langle\psi_0|T\{c_{k_2}(t_2)c_{k_1}^{\dagger}(t_1)\}|\psi_0\rangle,$$

where $c_k^{\dagger}(t)$ and $c_k(t)$ create and destroy a particle at time t, T is the Wick time-ordering operator, and ψ_0 is the exact normalized wave function of the ground state of the interacting N-particle system. These creation and destruction operators are in the 'Heisenberg picture' defined by

$$c_{k_1}^{\dagger}(t_1)=e^{iHt_1}c_{k_1}^{\dagger}e^{-iHt_1}$$

$$c_{k_2}^{\dagger}(t_2)=e^{iHt_2}c_{k_2}^{\dagger}e^{-iHt_2},$$

where H is the Hamiltonian of the interacting system. The Green's function propagator defined above destroys a particle at k_2, t_2, and creates a particle at k_1, t_1. Essentially, the Green's function propagator is a probability amplitude that the system will go from an initial state to a final state. The Green's function includes all intermediate states in the probability amplitude. Since there is an infinite number of possible intermediate states, the Green's function can end up representing an infinite series of possible states. Typically, instead of looking at this infinite number of

states, the series is transformed as a geometrical series into a single expression. This greatly simplifies the problem, but it still leaves the determination of the single expression.

To derive Dyson's equation, we will have to use methods that go beyond ordinary perturbation theory. This will require the infinite summation of possible states, many of these states are infinite. This geometric summation can be rewritten in such a way that is it possible to simplify the summation into a finite expression. This partial sum technique can be generalized to yield an extremely convenient exact expression for the propagator which is known as Dyson's equation. This sum is possible since we are only dealing with simple repeated parts of diagrams which are handing on the main directed $(\mathbf{k},\omega)$-line. These simple diagrams are bubbles, open oysters, rings, etc. which can be written without the main propagator line. Once we look at all possible cases that use these simple diagrams, the series is then summed into a finite form. If this sum is over all repetitions of all irreducible self-energy parts, we end up with Dyson's equation for a single particle. Translating Dyson's diagram into Green's function propagators, we end up with

$$G(\mathbf{k},\omega)=\frac{1}{\omega-\omega_k-\Sigma(\mathbf{k},\omega)+i\delta_k}.$$

In the above equation, $\Sigma(\mathbf{k},\omega)$ is related to the sum of all proper self-energy parts. Of course, for non-interacting systems, $\Sigma(\mathbf{k},\omega)=0$. Dyson's equation is the basic equation most propagator calculations start from. Of course, determining $\Sigma(\mathbf{k},\omega)$ is still very difficult, but the problem is simpler than trying to calculate the Green's function propagators for the entire infinite series of diagrams. Dyson's equation lets us simplify the problem immensely. Typically determining $\Sigma(\mathbf{k},\omega)$ is where the approximations come into play. Certain diagrams will dominate and only those are calculated, while the other less important diagrams are not calculated. It is important to note that Dyson's equation in this form is only valid when no external potentials exist, and the diagrams calculated are in $(\mathbf{k},\omega)$ space.

In the high-density electron gas, nearly the entire contribution to the self energy comes from the 'ring' diagrams('random phase approximation' or 'RPA'). This interaction can be interpreted as a 'screened' interaction between two particles. These rings are often called 'polarization diagrams' since they have one interaction line entering and one leaving the diagram. They show how the interaction causes the medium to become 'virtually polarized' in all possible ways. This approximation allows us to write the effective potential as

$$V_{eff(RPA)}(\mathbf{q},\omega) = \frac{V_q}{\varepsilon_{RPA}(\mathbf{q},\omega)},$$

where $\varepsilon_{RPA}(\mathbf{q},\omega)$ is the generalized dielectric constant. The dielectric properties of a medium arise because of the polarization of the medium by a field, and the sum of all ring diagrams represents the polarization of the electron gas by the field of one of the electrons in the gas itself.

The field theory related to this dissertation is discussed in Chapter 6. The theory starts out with Dyson's equation. From the optical theorem we know that the spectral function is related to the imaginary part of the green's function. In this case, the Green's function is for a collective excitation, and not a single particle excitation which was covered above. Similar to the single particle case, for the collective excitation, the Dyson's equation is given by

$$D(q,\omega) = \frac{1}{\omega^2 - \omega_0^2 - \Sigma(\mathbf{q},\omega)},$$

where D is the Dyson's Green's function, ω_0 is an undamped phonon frequency, and $\Sigma(\mathbf{q},\omega)$ is the exact self energy with no approximation. In this case, the important term to the self energy are the ring diagrams. Hence, we will approximate the self energy as

$$\Sigma(\mathbf{q},\omega) = |g(p)|^2 \Pi(\mathbf{q},\omega).$$

and all other contribution are considered to be non-important and ignored. In the above equations, $\Sigma(\mathbf{q},\omega)$ is the self energy which for this case has been approximated using only the simple ring diagrams, g(p) is the electron-phonon coupling constant, and $\Pi(\mathbf{q},\omega)$ is the irreducible polarizability. The problem arises in exactly how to determine $\Pi(\mathbf{q},\omega)$ which contains a very difficult integral. To perform this integral some assumptions must be made. Schuster extended the limits on integration out to infinity, while Varma made assumptions about the fermi surface to perform the integral. The results of these calculations are talked about in Chapter 6.

REFERENCES

1. For a review, see S. Roth, *Applied Physics*, **15**, 1 (1978).

2. For a review of magnetic superconductors as of 1990, see O. Fisher, *Ferromagnetic materials*, Vol. 5, ed. K.H.J. Bushow and E.P. Wohlfarth (North Holland, Amsterdam, 1990) P. 465.

3. G.K. Shenoy, B.D. Dunlap, F.Y. Fradin (eds.), Proc. Int. Conf. on Ternary Superconductors (North-Holland, Amsterdam, 1981).

4. M.B. Maple and O. Fischer (eds.), *Superconductivity in Ternary Compounds, Vols. I and II, Topics in Current Physics* (Springer, Berlin, Heidelberg and New York, 1982).

5. S.K. Sinha, H.A. Mook, O.A. Pringle, D.G. Hinks, in: Superconductivity in Magnetic and Exotic Materials: Proc. 6th Taniguchi Internat. Symp. Kashikojima, Japan, November 14-18, 1983, eds. T. Matsubara and A. Kotani, (Springer-Verlag, New York, 1984) pp. 14-28.

6. W.A. Fertig, D.C. Johnston, L.E. DeLong, R.W. McCallum, M.B. Maple, and B.T. Mattheis, *Phys. Rev. Lett.* **38**, 987 (1977).

7. D.E. Moncton, *J. Appl. Phys.* **50**(3), 1880 (1979).

8. D.E. Monctom, G. Shirane, and W. Thominson, *J. of Magnetism and Magnetic Materials* **14**, 172 (1979).

9. D.E. Monctom, D.B. MeWhan, P.H. Schmidt, G. Shirane, W. Thomlinson, M.B. Maple, H.B. MacKay, L.D. Woolf, Z. Fisk, and D.C. Johnston, *Phys. Rev. Lett.* **45**, 2060 (1980).

10. J.W. Lynn, G. Shirane, W. Thomlinson, and R.N. Shelton, *Phys. Rev. Lett.* **46**, 368 (1981).

11. S.K. Sinha, G.W. Crabtree, D.G. Hinks, and H. Mook, *Phys. Rev. Lett.* **48**, 950 (1982).

12. J.W. Lynn, J.A. Gotaas, R.W. Erwin, R.A. Ferrel, J.K. Bhattacharjee, R.N. Shelton, and P. Klavins, *Phys. Rev. Lett.* **52**, 133 (1984).

13. J.A. Gotaas, J.W. Lynn, R.N. Shelton, P. Klavins, and H.G. Braun, *Phys. Rev. B* **36**, 7277 (1987).

14. *Proceedings of the International Conference on Ternary Superconductors*, edited by G.K. Shernoy, B.D. Dunlap, and F.Y. Fradin (North-Holland, Amstardam, 1981).

15. *Superconductivity in Ternary Compounds, Vols, I and II of Topics in Current Physics*, edited by M.B. Maple, and O. Fisher (Springer, Berlin, 1982).

16. R. Nagarajan, C. Maxumundar, Z. Hosain, S.K. Dhar, K.V. Golparrishnan, L.C. Gupta,C. Godart, B.D. Pedalia, and R. Vijayaraghavan, *Phys. Rev. Lett.* **72**, 274, (1994).

17. R.J. Cava, H. Takagi, H.W. Zandbergen, H.H. Krajewski, W.F. Peck, Jr., T. Siegrist, B. Batloff, R.B. van Dover, R.J. Felder, K. Mizuhashi, J.O. Lee, H. Eisaki, and S. Uchida, *Nature* (London) **367**, 252 (1994).

18. T. Siegrist, H.W. Zandbergen, R.J. Cava, J.J. Krajewski, and W.F. Peck, Jr., *Nature* (London) **367**, 254 (1994).

19. R. Cava, H. Takagi, B. Batloff, H.W. Zndbergen, J.J. Krajewski, W.F. Peck, Jr., R.B. van Dover, R.J. Felder, T. Siegrist, K. Mizuhashi, J.O. Lee, H. Eisasi, S.A. Cater, and S. Uchida, *Nature* (London) **367**, 146 (1994).

20. Ming Xu, B.K. Cho, P.C. Canfield, D.K. finnemore, and D.C. Johnston, *Physica C* **235-240**, 2533 (1994).

21. Ming Xu, P.C. Canfield, J.E. Ostenson, D.K. Finnemore, B.K. Cho, Z.R. Wang, D.C. Johnston, *Physica C* **227**, 321 (1994).

22. B.K. Cho, Ming Xu, P.C. Canfield, L.L. Miller, and D.C. Johnston, *Phys. Rev. B* **52**, 3676 (1995).

23. B.K. Cho, P.C. Canfield, L.L. Miller, and D.C. Johnston, *Phys. Rev. B* **52**, 3684 (1995).

24. K.D.D. Rathnayaka, D.G. Naugle, B.K. Cho, P.C. Canfield, *Phys. Rev. B* **53**, 5688 (1996).

25. B.K. Cho, P.C. Canfield, and D.C. Johnston, *Phys. Rev. B* **52**, R3844, (1995).

26. P. Dervenagas, J. Zarestky, C. Stassis, A.I. Goldman, P.C. Canfield, B.K. Cho, *Physica B* **212**, 1 (1995).

27. P.C. Canfield, B.K. Cho, K.W. Dennis, *Physica B* **215**, 337 (1995).

28.B.K. Cho, P.C. Canfield, D.C. Johnston, *Phys. Rev. B* **53**, 8499 (1996).

29.C. Stassis and A. Goldman, *J. Alloys and Comp.* **250**, 603 (1997).

30.A.I. Goldman, C. Stassis, P.C. Canfield, J. Zarestky, P. Dervenagas, B.K. Cho, D. C. Johnston, And B. Sternlieb, *Phys. Rev B* **50**, 9668 (1995)

31.T.E. Grigereit, J.W. Lynn, Q. Huang, A. Santoro, *Phys. Rev. Lett.* **73**, 2756 (1994).

32.T. Vogt, A. Goldman, B. Sternlieb, and C. Stassis, *Phys. Rev. Lett.* **75**, 2628 (1995).

33.J. Zarestky, C. Stassis, A.I. Goldman, P.C. Canfield, P. Dervenagas, B.K. Cho, and D. C. Johnston, *Phys. Rev. B* **51**, 678 (1995).

34.S.K. Sinha, J.W. Lynn, T.E. Griegereit, Z. Hossain, L.C. Gupta, R. Nagarajan, and C. Godart, *Phys. Rev. B* **51**, 681 (1995).

35.C. Detlefs, A.I. Goldman, J.P. Hill, D. Gibbs, C. Stassis, P.C. Canfield, and B.K. Cho, *Phys. Rev. B* **53**, 6355 (1996).

36.P. Dervenagas, J. Zarestky, C. Stassis, A.I. Goldman, P.C. Canfield, and B.K. Cho, *Phys. Rev. B* **53**, 8506 (1995).

37.M.A. Ruderman, C. Kittel, *Phys. Rev.* **96**, 99 (1954).

38.T. Kasuya, *Progr. Theoret. Phys.*(Japan), **16**, 45 (1956).

39.K. Yosida, *Phys. Rev.* **106**, 893 (1957).

40.J.H. Van Vleck, *Rev. Mod. Phys.* **34**, 681 (1962).

41.J.M. Ziman, Principles of the Theory of Solids (Cambridge, 1972).

42.W. Kohn, *Phys. Rev. Lett.* **2**, 393 (1959).

43.B.N. Brockhose, T. Arase, G. Cagliota, K.R. Rao, and A.D.B. Woods, *Phys. Rev.* **128**, 1099 (1962).

44.J.Y. Rhee, X. Wang, and B.N. Harmon, *Phys. Rev. B* **51**, 15585 (1995).

45.J. Rath and A.J. Freeman, *Phys. Rev. B* **11**, 2109 (1975).

46.F. Gompf, W. Reichardt, H. Schober, B. Renker, M. Buchgeister, *Phys. Rev. B* **55**, 9058 (1997).

47.I.K. Yanson, V.V. Fisun, A.G.M. Jansen, P. Wyder, P.C. Canfield, B.K. Cho, C.V. Tomy, D. McK. Paul, *Phys. Rev. Lett.* **78**, 935 (1997).

48.H. Kwano, H. Yoshizawa, H. Takeya, K. Kadowaki, *Phys. Rev. Lett.* **77**, 4628 (1996).

49.M. Xu, P.C. Canfield, J.E. Ostenson, D.K. Finnemore, B.K. Cho, Z.R. Wang, and D.C. Johnston, *Physica C* **227**, 321 (1994).

50.B. Cho, *Anisotropic superconducting and normal state magnetic properties of single crystals of RNi2B2C compounds (R = Y,Gd,Dy,Ho,Er, and Tm)* (ISU Dissertation, 1995).

51.R. Celotta and J. Levine, Methods of Experimental Physics Vol 23-part A, (Academic Press, 1986).

52.G.E. Bacon, Neutron Diffraction (Clarendon Press, 1975).

53.H. Dachs, Neutron Diffraction (Springer Press, 1978).

54.P. Brüesch, Phonons: Theory and Experiments II (Springer Press, 1982).

55.P. Brüesch, Phonons: Theory and Experiments II (Springer Press, 1986).

56.P. Brüesch, Phonons: Theory and Experiments III (Springer Press, 1987).

57.J. Harada, J.D. Axe, G. Shirane, *Phys. Rev. B* **4**, 155, (1971).

58.J.D. Axe, J. Harada, G. Shirane, *Phys. Rev. B* **1**, 1227 (1970).

59.J.D. Axe and G. Shirane, *Phys. Rev. Lett.* **30**, 214 (1973).

60.S.M. Shapiro, G. Shirane, J.D. Axe, *Phys. Rev. B* **12**, 4899 (1975).

61.T. Ekino, H. Fujii, M. Kosugi, Y. Zenitani, J. Akimitsu, *Phys. Rev B* **53**, 9 (1996).

62.G.T. Jeong, J.I. Kye, S.H. Chun, Z.G. Khim, W.C. Lee, P.C. Canfield, B.K. Cho, D.C. Johnston, *Physica C*, **253**, 48 (1995).

63.N. Pyka, W. Reichardt, L. Pintschovius, G. Engel, J. Rossat-Mignod, J.Y. Henry, *Phys. Rev. Lett.* **70**, 1457 (1993).

64.H.A. Mook, B.C. Chakoumakos, M. Mostoller, *Phys. Rev. Lett.* **69**, 2272 (1992).

65.B. Friedl, C. Thomsen, M. Cardona, *Phys. Rev. Lett.* **65**, 915 (1990).

66.F. Marsiglio, *Phys. Rev. B* **47**, 5419 (1993).

67.M.V. Klein, S.B. Dierker, *Phys. Rev. B* **29**, 4976 (1984).

68.R. Zeyher and G. Zwicknagl, *Z Phys. B* **78**, 175 (1990).

69.P.B. Allen, V.N. Kostur, N. Takesue, and G. Shirane, *Phys. Rev. Lett.* -to be published.

70.H.Y. Kee and C.M. Varma(preprint)

71.H.G. Schuster *Solid State Comm.* **13**, 1559 (1973).

72.R. Zeyher, *Phys. Rev. B* **44**, 9596 (1991).

73.J.M. Ziman, Principles of the theory of Solids (Cambridge University Press, 972).

74.R.D. Mattuck, A Guide to Feynman diagrams in the many-body problem (McGraw-Hill Internationsl Book Company, 1976).